Article

Cell Reports

Innate Immunity in the *C. elegans* Intestine Is Programmed by a Neuronal Regulator of AWC Olfactory Neuron Development

Graphical Abstract

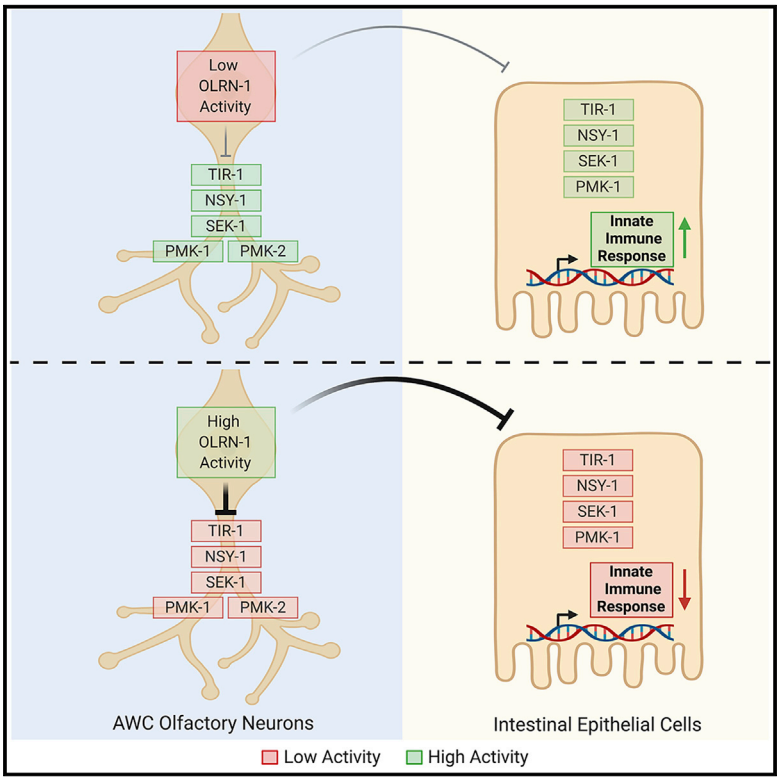

Authors

Kyle J. Foster, Hilary K. Cheesman, Pengpeng Liu, Nicholas D. Peterson, Sarah M. Anderson, Read Pukkila-Worley

Correspondence

read.pukkila-worley@umassmed.edu

In Brief

During nematode development, the olfactory neuron gene *olrn-1* programs odorant receptor expression in AWC neurons. Foster et al. show that *olrn-1* also functions in AWC neurons to suppress innate immune defenses in the intestine. These data reveal an unexpected connection between olfactory receptor development and innate immunity.

Highlights

- The olfactory neuron gene *olrn-1* regulates intestinal immunity in *C. elegans*
- Neuronal *olrn-1* suppresses the p38 MAPK PMK-1 immune pathway in the intestine
- Promotion of immune homeostasis by *olrn-1* ensures evolutionary fitness
- *olrn-1*-dependent immune effectors are dynamically regulated during development

Foster et al., 2020, Cell Reports *31*, 107478
April 7, 2020
https://doi.org/10.1016/j.celrep.2020.03.042

CellPress

Cell Reports
Article

Innate Immunity in the *C. elegans* Intestine Is Programmed by a Neuronal Regulator of AWC Olfactory Neuron Development

Kyle J. Foster,[1] Hilary K. Cheesman,[1] Pengpeng Liu,[2] Nicholas D. Peterson,[1] Sarah M. Anderson,[1] and Read Pukkila-Worley[1,2,3,*]

[1]Program in Innate Immunity, Division of Infectious Diseases and Immunology, University of Massachusetts Medical School, Worcester, MA 01655, USA

[2]Department of Molecular, Cell and Cancer Biology, University of Massachusetts Medical School, Worcester, MA 01655, USA

[3]Lead Contact

*Correspondence: read.pukkila-worley@umassmed.edu

https://doi.org/10.1016/j.celrep.2020.03.042

SUMMARY

Olfactory neurons allow animals to discriminate nutritious food sources from potential pathogens. From a forward genetic screen, we uncovered a surprising requirement for the olfactory neuron gene *olrn-1* in the regulation of intestinal epithelial immunity in *Caenorhabditis elegans*. During nematode development, *olrn-1* is required to program the expression of odorant receptors in the AWC olfactory neuron pair. Here, we show that *olrn-1* also functions in AWC neurons in the cell non-autonomous suppression of the canonical p38 MAPK PMK-1 immune pathway in the intestine. Low activity of OLRN-1, which activates the p38 MAPK signaling cassette in AWC neurons during larval development, also de-represses the p38 MAPK PMK-1 pathway in the intestine to promote immune effector transcription, increased clearance of an intestinal pathogen, and resistance to bacterial infection. These data reveal an unexpected connection between olfactory receptor development and innate immunity and show that anti-pathogen defenses in the intestine are developmentally programmed.

INTRODUCTION

The expression of a diverse array of olfactory receptors within sensory neurons is essential for metazoans to survive in microbe-rich environments. For example, amphid neurons in the head of the nematode *C. elegans* sample the environment and program rapid changes in locomotion, which allows nematodes to forage decomposing organic matter for bacterial food sources and avoid potential pathogens. Thus, *C. elegans* provides an experimental platform to understand how the development of sensory neurons is integrated with the physiology of the organism as a whole.

In addition to learned behavioral aversion responses to bacterial pathogens, innate immune defenses in intestinal epithelial cells allow nematodes to survive challenge from environmental pathogens (Kim and Ewbank, 2018; Pukkila-Worley, 2016). The canonical immune pathway in intestinal cells is anchored by the p38 mitogen-activated protein kinase (MAPK) PMK-1 (Kim et al., 2002; Troemel et al., 2006). p38 MAPK PMK-1 functions as part of a classical MAPK signaling cassette, which is activated by MAPKKK NSY-1 and MAPKK SEK-1, homologs of mammalian ASK1 and MKK3/6, respectively (Kim et al., 2002), and by TIR-1, a toll/interleukin-1 receptor (TIR) domain protein (Liberati et al., 2004). The p38 MAPK PMK-1 pathway ensures the basal expression of immune effectors in the absence of a pathogen (Peterson et al., 2019; Troemel et al., 2006). Thus, mechanisms that adjust basal levels of p38 MAPK PMK-1 pathway activity could act as a rheostat for immune effector expression, functioning both to prime *C. elegans* intestinal epithelial cells for the induction of anti-pathogen responses and to limit the deleterious effects of immune hyperactivation.

Here, we conducted a forward genetic screen to identify endogenous regulators of the p38 MAPK PMK-1 pathway. Genetic analyses of mutants identified in this screen uncovered a signaling axis between amphid wing C (AWC) sensory neurons and the intestinal epithelium that promotes immune homeostasis by suppressing the canonical p38 MAPK PMK-1 immune pathway. Interestingly, *olrn-1*, the newly discovered neuronal regulator of this pathway, was previously shown to control the expression of olfactory receptors in AWC sensory neurons (Bauer Huang et al., 2007). During neuronal development, *olrn-1* acts cell autonomously in AWC neurons to suppress the TIR-1/NSY-1/SEK-1 cassette, which signals redundantly through the p38 MAPK PMK-1 or PMK-2 (Bauer Huang et al., 2007; Chuang and Bargmann, 2005; Pagano et al., 2015; Troemel et al., 1999). Modulation of p38 MAPK pathway activity by OLRN-1 in AWC neurons leads to differentiation of olfactory receptor expression, a developmental step that is required for *C. elegans* to detect specific chemoattractive odors (Wes and Bargmann, 2001). We show that neuronal *olrn-1* also functions cell non-autonomously to suppress the p38 MAPK PMK-1 innate immune pathway in the intestine. Low *olrn-1* activity in AWC neurons, as recapitulated in multiple *olrn-1* loss-of-function mutant strains, de-represses the p38 MAPK PMK-1 pathway in the intestine, which promotes immune effector transcription, increased clearance of an intestinal pathogen, and resistance to bacterial infection. Interestingly, *olrn-1* and p38

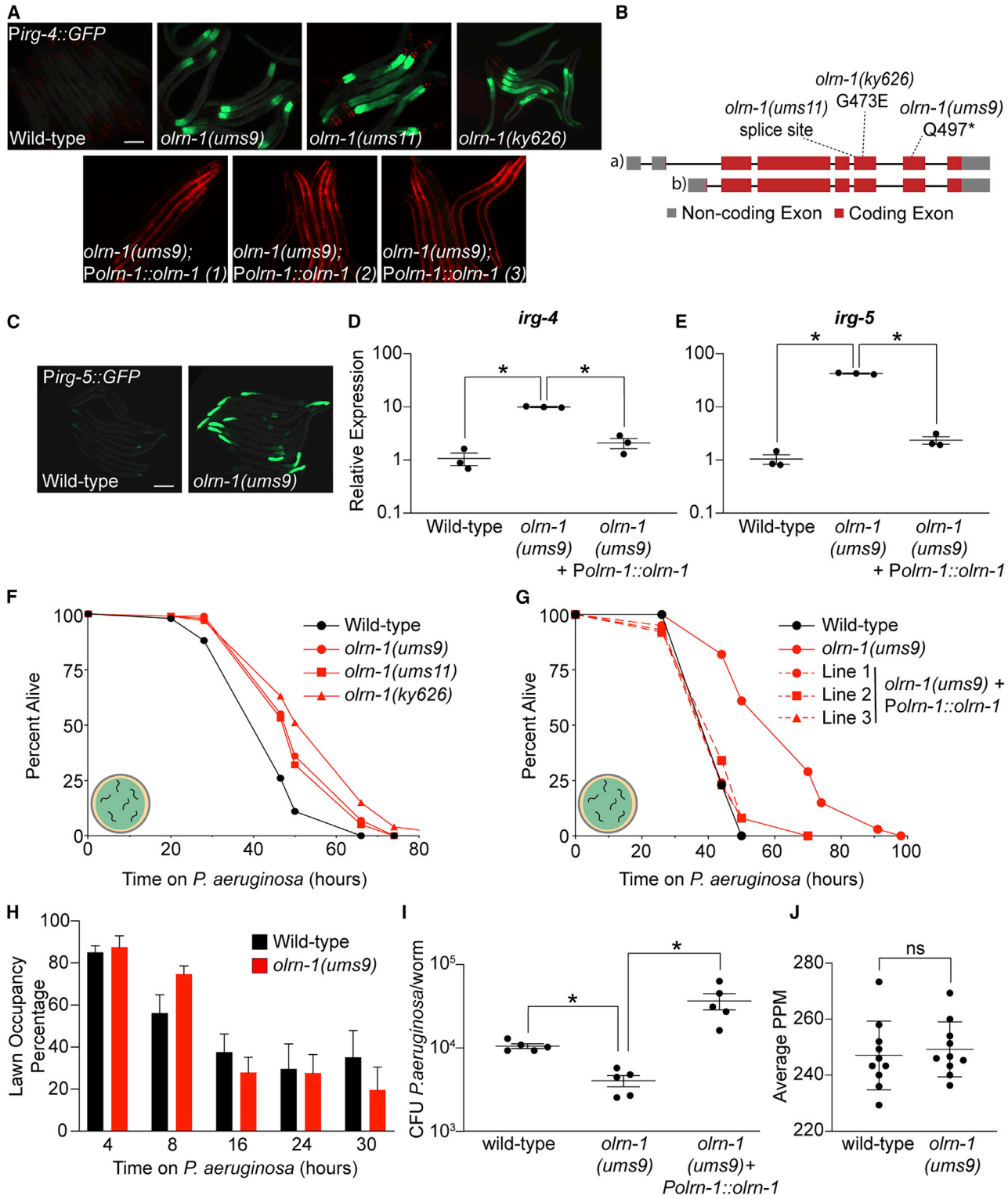

Figure 1. Loss-of-Function Mutations in *olrn-1* Cause Constitutive Immune Activation

(A) Images of *olrn-1* mutants and three independent rescue lines with *olrn-1* expressed under the control of its own promoter in the P*irg-4::GFP* immune reporter background are shown. Red pharyngeal expression is the P*myo-2::mCherry* co-injection marker, which confirms the presence of the P*irg-4::GFP* transgene. The P*myo-3::mCherry* co-injection marker confirms expression of the P*olrn-1::olrn-1* construct in the rescue lines.

(B) Schematic of the *olrn-1* locus with the locations of the *ums9*, *ums11*, and *ky626* mutations is shown.

(legend continued on next page)

MAPK *pmk-1*-dependent immune effectors are enriched among genes that are induced during larval development in wild-type nematodes. These data suggest that low activity of neuronal OLRN-1 de-represses the p38 MAPK PMK-1 pathway to prime the immune response in the intestine to handle challenges from bacterial pathogens encountered during larval development.

RESULTS

Loss-of-Function Mutations in *olrn-1* Cause Constitutive Immune Activation

We conducted a forward genetic screen to identify endogenous regulators of the p38 MAPK PMK-1 innate immune pathway. The innate immune reporter P*irg-4*(F08G5.6)::GFP was used for this experiment to provide a convenient readout of innate immune activation (Pukkila-Worley et al., 2014). *irg-4* is a putative *C. elegans* immune effector whose basal expression is under the control of the p38 MAPK PMK-1 innate immune pathway (Anderson et al., 2019; Peterson et al., 2019; Pukkila-Worley et al., 2012; Troemel et al., 2006). In addition, *irg-4* is upregulated during infection by multiple bacterial pathogens and is required for host defense against the bacterial pathogen *Pseudomonas aeruginosa* (Anderson et al., 2019; Nandakumar and Tan, 2008; Peterson et al., 2019; Shapira et al., 2006; Troemel et al., 2006). Previously, we screened the F1 progeny of mutagenized P*irg-4::GFP* animals for dominant mutations that cause constitutive immune activation and identified *nsy-1(ums8)*, a gain-of-function mutation in the MAPKKK that functions upstream of p38 MAPK *pmk-1* (Cheesman et al., 2016). Thus, this approach can identify mutations that affect the activity of the p38 MAPK PMK-1 pathway.

To identify regulators of immune activation in *C. elegans*, we screened the F2 progeny of approximately 40,000 mutagenized P*irg-4::GFP* haploid genomes for recessive mutations that caused constitutive P*irg-4::GFP* expression, and we identified two mutant alleles: *ums9* and *ums11* (Figure 1A). Whole-genome sequencing of pooled F2 recombinants, homozygous for the mutant phenotype following two outcrosses to wild-type N2 animals, was performed to identify the mutations that caused constitutive P*irg-4::GFP* expression. Sequencing revealed that both *ums9* and *ums11* contain different recessive mutations in *olrn-1*, a neuronally expressed protein with putative transmembrane domains (Bauer Huang et al., 2007; Torayama et al., 2007). *ums9* is a nonsense mutation (Q497*), and *ums11* is a mutation that disrupts an *olrn-1* splice acceptor site (Figure 1B).

Several experiments demonstrated that loss-of-function mutations in *olrn-1* cause constitutive activation of P*irg-4::GFP*. First, expression of *olrn-1* under the control of its own promoter in three independent extrachromosomal arrays rescued the constitutive activation of P*irg-4::GFP* in the *ums9* mutant (Figure 1A). A previously characterized loss-of-function allele, *olrn-1(ky626)* (a missense mutation [G473E]), also caused constitutive activation of P*irg-4::GFP* (Figures 1A and 1B; Bauer Huang et al., 2007). Finally, we outcrossed *olrn-1(ums9)* to wild type six times and confirmed that P*irg-4::GFP* was still constitutively activated (Figure 1A).

A second transcriptional reporter for a different innate immune effector, P*irg-5*(F35E12.5)*::GFP*, is also constitutively activated in the intestine of *olrn-1(ums9)* mutants (Figure 1C). Like *irg-4*, *irg-5* is an immune effector that is required for host defense during *P. aeruginosa* infection and is a target of the p38 MAPK PMK-1 pathway (Bolz et al., 2010; Peterson et al., 2019; Troemel et al., 2006). Altogether, *irg-4* and *irg-5* are useful readouts of innate immune activation in the *C. elegans* intestine. Endogenous *irg-4* and *irg-5* were transcriptionally induced to comparable levels in *olrn-1(ums9)*, *olrn-1(ums11)*, and *olrn-1(ky626)* mutants, and reintroduction of *olrn-1* under the control of its own promoter rescued the constitutive activation of these genes in the *olrn-1(ums9)* mutant background (Figures 1D, 1E, and S1A–S1C).

Consistent with the constitutive activation of innate immune effector transcription in *olrn-1* loss-of-function animals, *olrn-1* mutants displayed increased resistance to infection by *P. aeruginosa* (Figure 1F). Importantly, we confirmed that loss of function of *olrn-1* modulates the susceptibility of *C. elegans* to *P. aeruginosa* infection by testing the pathogen susceptibility of the three independent *olrn-1* rescue lines described earlier (Figure 1G). Expression of *olrn-1* under the control of its own promoter rescued the pathogen-resistance phenotype of the *olrn-1(ums9)* mutant (Figure 1G). We considered that *olrn-1* mutants may be resistant to *P. aeruginosa* infection because they are better able to avoid the pathogen than wild-type animals. However,

(C) Immune reporter P*irg-5::GFP* in the *olrn-1(ums9)* background is shown.

(D and E) Presence of the P*irg-5::GFP* transgene was confirmed by assaying for the RoI phenotype. qRT-PCR data of *irg-4* (D) and *irg-5* (E) of the indicated genotypes is presented. Data are the average of three independent replicates, each normalized to a control gene, with error bars representing SEM, Data are presented as the value relative to the average expression from all replicates of the indicated gene in wild-type animals. *$p < 0.05$ by one-way ANOVA for the indicated comparison.

(F and G) *C. elegans* pathogenesis assay conducted with a large lawn of *P. aeruginosa* and *C. elegans* of indicated genotypes at L4 is shown. Data are representative of three trials. The Kaplan-Meier method was used to estimate the survival curves for each group, and the log rank test was used for all statistical comparisons. Sample sizes, mean lifespan, and p values for all trials are shown in Table S2.

(H) Quantification of the propensity of *olrn-1(ums9)* and wild-type animals to avoid a lawn of *P. aeruginosa* is shown. Data are presented as the average number of animals that were on a small lawn of *P. aeruginosa* from three separate replicates, with error bars representing SEM. There is no significant difference by one-way ANOVA between these mutants, except at the 8-h time point.

(I) *P. aeruginosa*, isolated from the intestines of animals with the indicated genotypes, was quantified after 24 h of bacterial infection. Data are colony-forming units (CFUs) of *P. aeruginosa* and are presented as the average of five separate replicates, with each replicate containing 10–11 animals. *$p < 0.05$ by one-way ANOVA for the indicated comparison.

(J) Data are the pharyngeal pumping rates, recorded as pumps per minute (PPM), of 10 individual young adult *C. elegans* feeding on non-pathogenic OP50 in wild-type and *olrn-1(ums9)* mutants, with error bars representing SEM. ns indicates no significant difference by one-way ANOVA for the indicated comparison.
Scale bars in (A) and (C) are 100 μm. See also Figure S1.

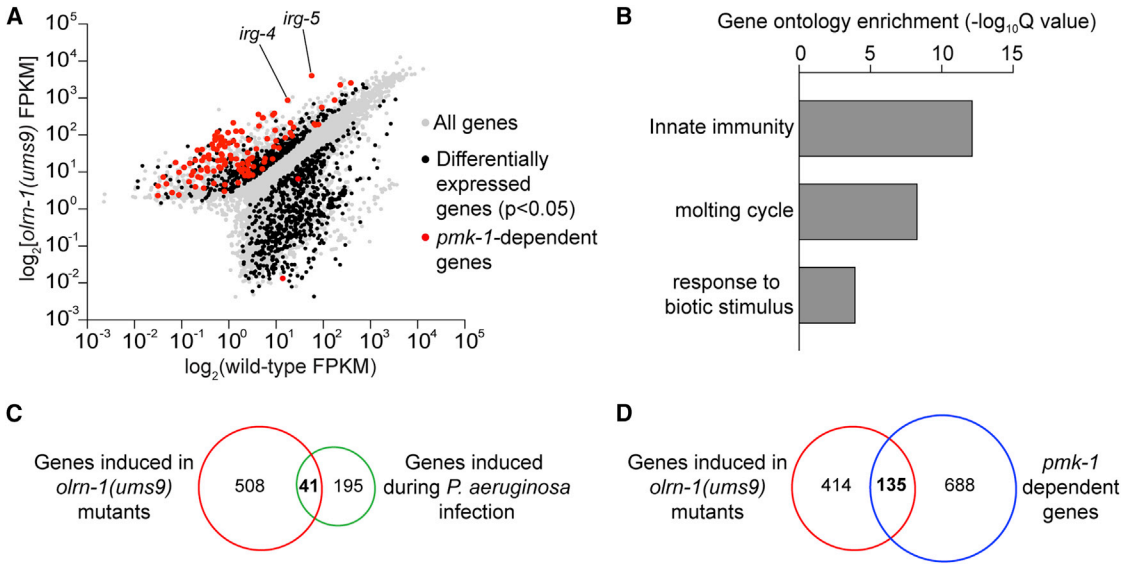

Figure 2. *olrn-1* Suppresses Innate Immune Effector Expression

(A) Data from an mRNA sequencing (mRNA-seq) experiment comparing gene expression in *olrn-1(ums9)* mutants with wild-type animals are shown. All genes are shown in gray. Genes that are differentially expressed in *olrn-1(ums9)* mutants compared with wild-type animals are shown in black (fold change > 2, $p < 0.05$). Genes that are known targets of the p38 MAPK *pmk-1* pathway are highlighted in red. The locations of the representative genes *irg-4* and *irg-5*, whose expression is examined throughout this manuscript, are shown.

(B) Gene Ontology enrichment analysis for the 549 genes whose transcription was significantly upregulated in *olrn-1(ums9)* mutants compared with wild type is shown. The three most significantly enriched categories are shown, reported as the $-\log_{10}$ transformation of the Q value for the enrichment of each category.

(C and D) Venn diagrams show the overlap of the 549 genes upregulated in *olrn-1* mutants with genes that are known to be induced during *P. aeruginosa* infection (C) and are targets of the p38 MAPK PMK-1 pathway (D). Hypergeometric p values for the overlap in (C) and (D) are 3.22e−21 and 9.10e−67, respectively. See also Figure S2.

olrn-1(ums9), *olrn-1(ums11)*, and *olrn-1(ky626)* mutants were resistant to *P. aeruginosa* infection in a pathogenesis assay conducted with a lawn of bacteria that was spread to the edges of the agar, which negates the contribution of behavioral avoidance to the pathogen-resistance phenotype (Figure 1F; Reddy et al., 2009; Styer et al., 2008; Sun et al., 2011). In addition, the *olrn-1(ums9)* mutant did not have increased propensity to avoid a small lawn of *P. aeruginosa* compared with wild type (Figure 1H).

The *olrn-1(ums9)* mutant animals accumulated significantly less *P. aeruginosa* in their intestines compared with wild-type animals (Figure 1I). Reintroduction of *olrn-1* under the control of its own promoter complemented this *olrn-1(ums9)* mutant phenotype (Figure 1I). There was no difference in pharyngeal pumping rates between wild-type and *olrn-1(ums9)* mutants (Figure 1J). In addition, *olrn-1(ums9)* and *olrn-1(ky626)* mutants each have a lifespan that is similar to that of wild-type animals (Figure S1D). Altogether, these data demonstrate that *olrn-1(ums9)* mutants drive a transcriptional response that promotes clearance of bacteria from the intestine and resistance to *P. aeruginosa* infection, without pleiotropic effects on feeding behavior or nematode lifespan.

olrn-1 Suppresses the p38 MAPK PMK-1 Innate Immune Pathway

To characterize the full spectrum of genes regulated by *olrn-1*, we performed RNA sequencing (RNA-seq). The transcriptomes of wild-type and *olrn-1(ums9)* mutant animals growing in standard culture conditions (i.e., in the absence of pathogen challenge) were profiled. In *olrn-1(ums9)* mutants, 549 genes were upregulated compared with wild type (greater than 2-fold, $p < 0.05$) (Figure 2A; Table S1). Analysis of these differentially expressed transcripts revealed significant enrichment for innate immune genes (Figure 2B), including *irg-4* and *irg-5* (Figure 2A). Indeed, 41 of the 236 genes that are induced during pseudomonal infection (Miller et al., 2015) are also constitutively upregulated in the *olrn-1(ums9)* mutant (hypergeometric p value 3.22e−21) (Figure 2C).

Loss-of-function *olrn-1* mutants demonstrated constitutive activation of P*irg-4::GFP* (Figure 1A) and P*irg-5::GFP* (Figure 1C) in the intestinal epithelial cells of *C. elegans*, the tissue that directly interfaces with ingested pathogens. In the RNA-seq experiment, 171 of the 549 *olrn-1*-repressed genes are expressed in intestinal epithelial cells (hypergeometric p value 1.16e−32) (Haenni et al., 2012). Altogether, these data indicate that *olrn-1* suppresses the transcription of genes that are expressed in the intestine, which includes a significant number of immune effectors.

The RNA-seq experiment also revealed that *olrn-1* negatively regulates a significant number of genes that are known targets of the p38 MAPK PMK-1 pathway (Bond et al., 2014; Troemel et al., 2006). Of the 549 genes that are upregulated in *olrn-1(ums9)* mutants, 135 depend on *pmk-1* for their basal transcription (hypergeometric p value 9.10e−67) (Figures 2A and 2D; Bond et al., 2014). To determine whether *olrn-1* controls the activity of the p38 MAPK PMK-1 pathway, we performed western blot experiments with antibodies that recognize the doubly

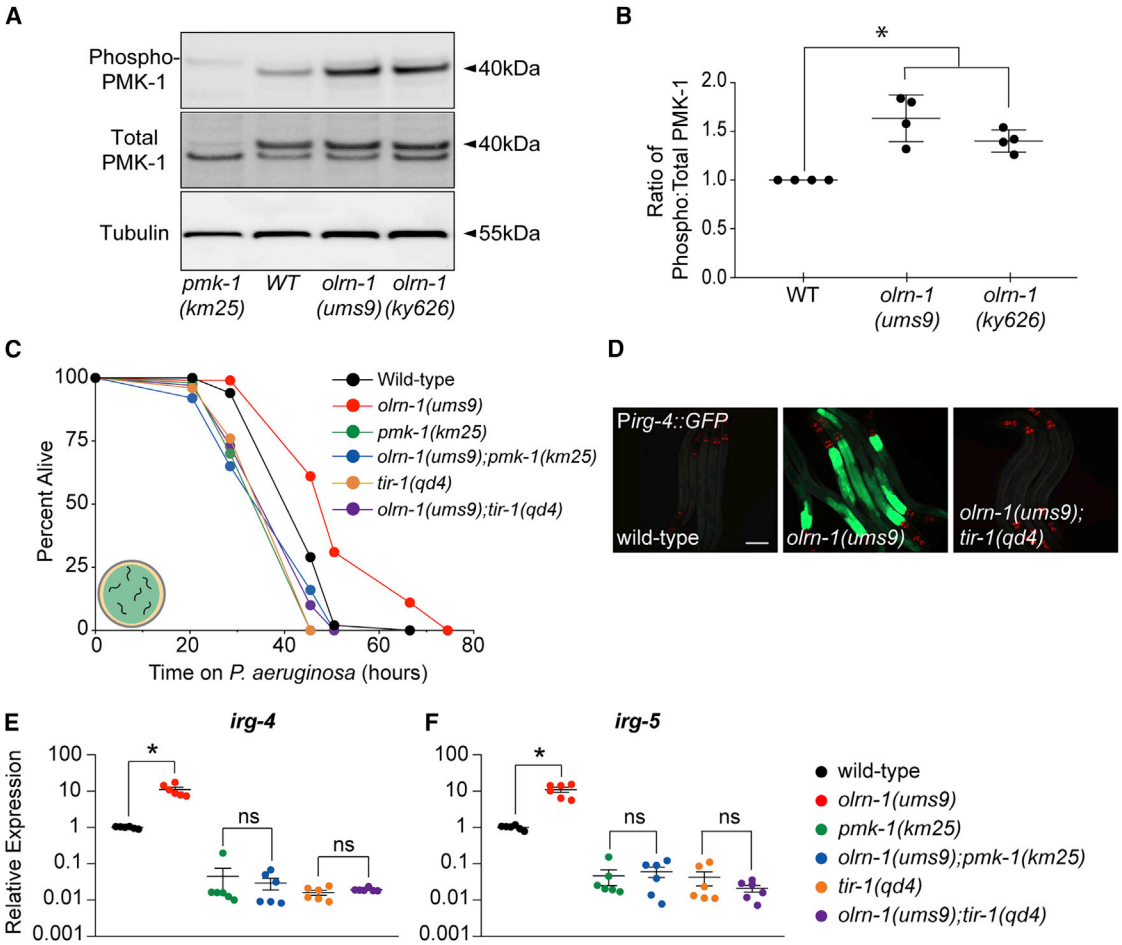

Figure 3. *olrn-1* Suppresses the p38 MAPK PMK-1 Innate Immune Pathway

(A) Immunoblot analysis of lysates from animals of the indicated genotype using antibodies that recognize the doubly phosphorylated TGY motif of PMK-1 (phospho-PMK-1), the total PMK-1 protein (total PMK-1), and tubulin is shown. PMK-1 is a 40 kDa protein, and tubulin is a 55 kDa protein.

(B) Band intensities of four biological replicates of the western blot shown in (A) were quantified. The ratio of active to total PMK-1 is shown for each genotype and is presented relative to the ratio in wild-type animals for each replicate. *$p < 0.05$ by one-way ANOVA for the indicated comparison.

(C) *C. elegans* pathogenesis assay conducted with a large lawn of *P. aeruginosa* and *C. elegans* of indicated genotypes at L4 is shown. Data are representative of three trials. The Kaplan-Meier method was used to estimate the survival curves for each group, and the log rank test was used for all statistical comparisons. Sample sizes, mean lifespan, and p values for all trials are shown in Table S2.

(D) Images of *olrn-1(ums9)* mutants and *olrn-1(ums9);tir-1(qd4)* double mutants are shown. Red pharyngeal expression is the P*myo-2::mCherry* co-injection marker, which confirms the presence of the P*irg-4::GFP* transgene. Scale bar is 100 μm.

(E and F) qRT-PCR data show *irg-4* (E) and *irg-5* (F) expression in the indicated genotypes. Data are the average of six independent replicates, each normalized to a control gene, with error bars representing SEM. Data are presented as the value relative to the average expression from all replicates of the indicated gene in wild-type animals. *$p < 0.05$ by one-way ANOVA for the indicated comparison. ns denotes that the difference between the indicated comparisons was not statistically significant.

phosphorylated TGY motif of activated PMK-1 and the total PMK-1 protein. Both the *olrn-1(ums9)* and the *olrn-1(ky626)* loss-of-function mutants have an increased ratio of phosphorylated PMK-1 relative to total PMK-1 compared with wild-type controls, as quantified from four biological replicates (Figures 3A and 3B).

Consistent with these data, loss-of-function mutations in p38 MAPK PMK-1 pathway components *pmk-1(km25)* and *tir-1(qd4)* suppressed the pathogen-resistance phenotype of the *olrn-1(ums9)* mutants (Figure 3C). In addition, both *tir-1(qd4)* (Figure 3D) and *sek-1(km4)* (Figure 6A) suppressed the hyperactivation of P*irg-4::GFP* in the intestinal epithelial cells of the *olrn-1(ums9)* mutant. Moreover, *tir-1(qd4)* and *pmk-1(km25)* mutations each suppressed the constitutive activation of the immune effectors *irg-4* (Figure 3E) and *irg-5* (Figure 3F) in the *olrn-1(ums9)* background.

The bZIP transcription factor ZIP-2 and the G protein-coupled receptor FSHR-1 each function in parallel to the p38 MAPK PMK-1 pathway to promote host defense during an intestinal infection with *P. aeruginosa* (Estes et al., 2010; Powell et al., 2009; Reddy et al., 2016). Loss-of-function mutants of *zip-2* and *fshr-1* are hypersusceptible to killing by *P. aeruginosa* and

are unable to upregulate a suite of PMK-1-independent immune effectors (Estes et al., 2010; Powell et al., 2009; Reddy et al., 2016). We examined the genes that are transcriptionally upregulated in the *olrn-1(ums9)* mutants to determine whether *olrn-1* also suppresses the ZIP-2 or the FSHR-1 pathway. However, the overlap of *zip-2*-regulated genes (Figure S2A) or *fshr-1*-regulated genes (Figure S2B) with the genes that were upregulated in the *olrn-1(ums9)* mutant was not significant. In addition, we found that targets of the FOXO transcription factor DAF-16 were not significantly over-represented among *olrn-1*-regulated genes (Figure S2C).

Altogether, these data demonstrate that OLRN-1 targets the p38 MAPK PMK-1 immune pathway to suppress immune effector expression in the intestine and modulate host susceptibility to bacterial infection.

Promotion of Intestinal Immune Homeostasis by *olrn-1* Is Required to Ensure Reproduction and Development

We previously observed that aberrant activation of immune defenses in the intestine by a gain-of-function mutation in the p38 MAPKKK *nsy-1* (*nsy-1(ums8)*) or by exogenous treatment with an immunostimulatory small molecule slows nematode development (Cheesman et al., 2016). Like *nsy-1(ums8)* mutants, *olrn-1(ums9)* mutants take a longer time to reach adulthood than wild-type animals (Figures 4A and 4B). Reintroduction of *olrn-1* under the control of its own promoter restored wild-type developmental rates to the *olrn-1(ums9)* mutant (Figures 4A and 4B).

To determine whether the developmental delay in the *olrn-1(ums9)* mutant is a consequence of de-repression of the p38 MAPK PMK-1 pathway, we compared the developmental rates of the *pmk-1(km25)*, *tir-1(qd4)*, *atf-7(qd22 qd130)*, and *olrn-1(ums9)* single mutants to the *olrn-1(ums9);pmk-1(km25)*, the *olrn-1(ums9);tir-1(qd4)*, and the *olrn-1(ums9);atf-7(qd22 qd130)* double mutants (Figures 4G, 4H, and S3). ATF-7 is the transcription factor that functions downstream of p38 MAPK PMK-1 to control the basal expression of immune effectors (Shivers et al., 2010). The *pmk-1(km25)*, *tir-1(qd4)*, and *atf-7(qd22 qd130)* null mutants each fully suppressed the developmental delay of the *olrn-1(ums9)* mutant (Figures 4G, 4H, and S3). In addition, the brood sizes of both *nsy-1(ums8)* gain-of-function mutants and *olrn-1(ums9)* mutants are significantly smaller than those of wild-type animals (Figure 4I). Consistent with our observations in the *C. elegans* development experiments, both *pmk-1(km25)* and *tir-1(qd4)* mutations fully suppressed the small brood sizes of *olrn-1(ums9)* mutants (Figure 4I). Thus, neuronal *olrn-1* prevents the deleterious effects of aberrant immune activation on nematode development and reproductive fitness.

Expression of *olrn-1* in Chemosensory Neurons Is Sufficient to Regulate Innate Immunity in the Intestinal Epithelium

OLRN-1 is expressed in AWC chemosensory neurons, where it acts cell autonomously to promote olfactory receptor expression during nematode development (Bauer Huang et al., 2007). However, OLRN-1 is not expressed in the intestinal epithelium (Bauer Huang et al., 2007), where the p38 MAPK PMK-1 pathway coordinates the tissue autonomous expression of immune effectors and resistance to pathogen infection (Shivers et al., 2009). Therefore, we hypothesized that OLRN-1 acts in sensory neurons to control p38 MAPK PMK-1 transcriptional responses in the intestine.

We introduced an extrachromosomal array containing *olrn-1* under the control of a pan-neuronal promoter (P*sng-1::olrn-1*) into the *olrn-1(ums9)* mutant. Neuronal expression of *olrn-1* in three independent lines rescued the constitutive expression of P*irg-4::GFP* in the intestine of *olrn-1(ums9)* mutants (Figure 5A). We confirmed that neuronal expression of *olrn-1* was sufficient to suppress the constitutive activation of endogenous *irg-4* (Figure 5B) and *irg-5* (Figure 5C) in the *olrn-1(ums9)* mutant. Consistent with these gene expression data, neuronal expression of *olrn-1* in three independent lines suppressed the pathogen-resistance phenotype of the *olrn-1(ums9)* mutant (Figure 5D).

We also expressed *olrn-1* in the *olrn-1(ums9)* mutant under the *odr-3* promoter (P*odr-3::olrn-1*), which drives gene expression in a specific subset of chemosensory neurons (Roayaie et al., 1998). A P*odr-3::GFP* transcription reporter is expressed strongly in AWC neurons and weakly or inconsistently in AWB, AWA, ASH, and ADF neurons (Roayaie et al., 1998). Historically, the *odr-3* promoter has been a useful tool to characterize AWC-dependent mechanisms (Bauer Huang et al., 2007). As observed in our experiments with the P*sng-1::olrn-1* constructs (Figure 5D), expression of *olrn-1* under the *odr-3* promoter fully suppressed the pathogen-resistance phenotype of the *olrn-1(ky626)* mutant (Figure 5E). Importantly, this experiment, which uses a second heterologous promoter to direct *olrn-1* expression in neurons, confirms that *olrn-1* activity in neurons is necessary to modulate resistance to a bacterial pathogen. Multi-copy expression of *olrn-1* in a wild-type background, both under its own promoter and specifically in neurons, rendered *C. elegans* more susceptible to killing by *P. aeruginosa* (Figure 5F).

In addition, expression of *olrn-1* only in neurons (under the *sng-1* promoter) (Figures 4C and 4D) or in chemosensory neurons (using the *odr-3* promoter) (Figures 4E and 4F) was sufficient to rescue the developmental delay of *olrn-1* mutants, as assessed in multiple independent lines carrying these rescue constructs.

In summary, neuronal *olrn-1* is necessary and sufficient to control pathogen resistance and promote intestinal immune homeostasis. In addition, we show that expression of *olrn-1* in chemosensory neurons is sufficient to regulate innate immunity in the *C. elegans* intestinal epithelium.

Immune Effectors Regulated by Neuronal *olrn-1* Are Dynamically Expressed during Nematode Development

During *C. elegans* development, *olrn-1* suppresses the TIR-1/NSY-1/SEK-1 cassette in AWC neurons, which uses either PMK-1 or PMK-2 p38 MAPK to promote left-right asymmetry of the odorant receptors *str-2* and *srsx-3* in AWC neurons (Bauer Huang et al., 2007; Chuang and Bargmann, 2005; Pagano et al., 2015; Torayama et al., 2007; Troemel et al., 1999). Differentiation of odorant receptors in AWC neurons is a required developmental step for *C. elegans* to sense and move toward diverse attractive stimuli (Wes and Bargmann, 2001). Adult *C. elegans* have one AWC neuron that expresses *str-2*, called AWC^{ON} by convention, and one AWC neuron that expresses the *srsx-3* chemoreceptor instead (AWC^{OFF}). Forward genetic screens for mutants with two AWC^{ON} or two AWC^{OFF} neurons defined the

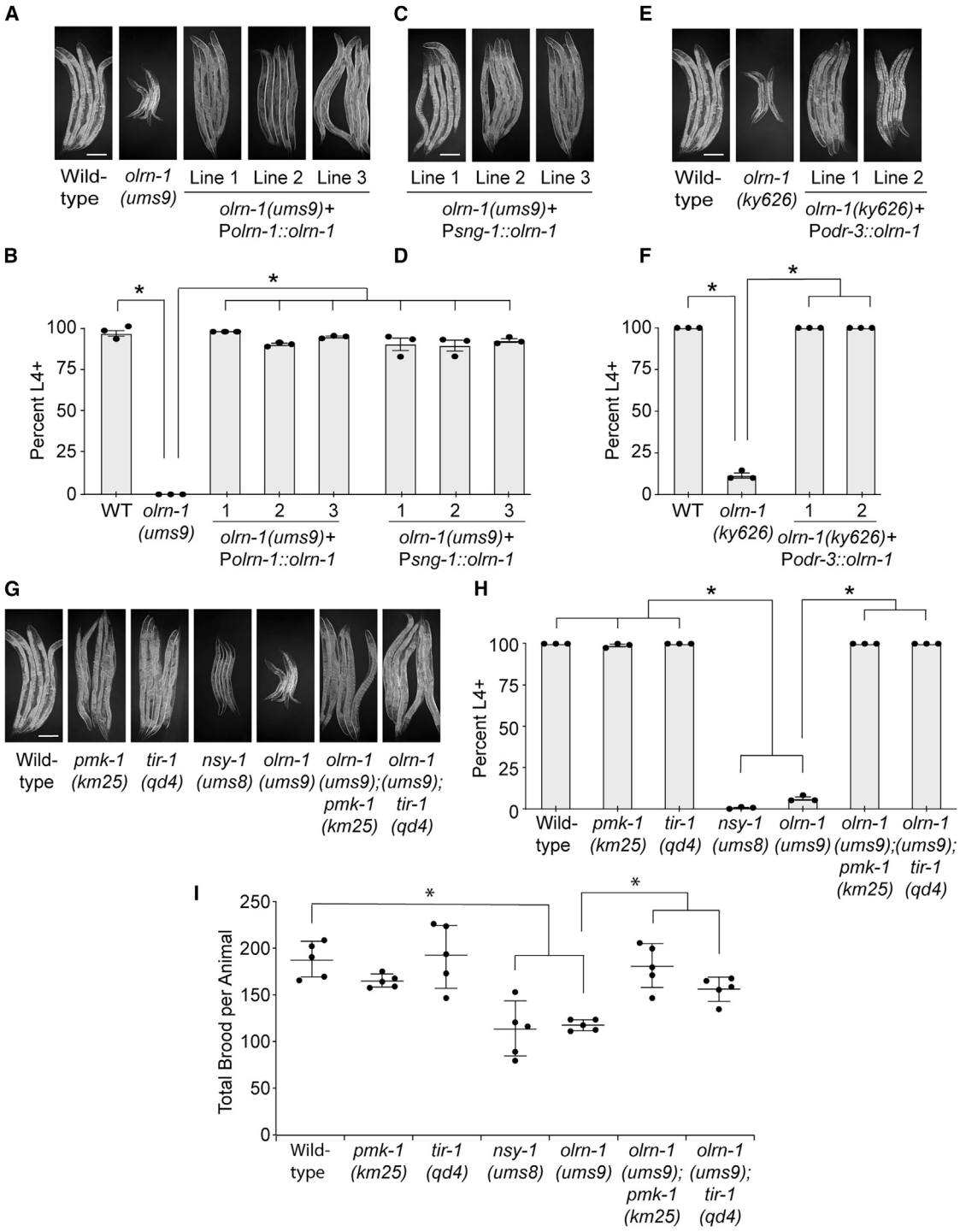

Figure 4. Promotion of Intestinal Immune Homeostasis by *olrn-1* Is Required to Ensure Reproduction and Development

(A–H) Development assays were performed with the indicated genotypes. The stage of the animals was recorded at the same time point, approximately 72 h after eggs from *C. elegans* of the indicated genotypes were laid. In (B), (D), (F), and (H), data are presented as the average number of animals for each genotype that were at L4 or older (percent L4+) from three independent replicates, with error bars representing SEM. *$p < 0.05$ by one-way ANOVA. The stage that was recorded for each animal in these assays and the sample size for all replicates are presented in Table S2. The animals in (A), (C), (E), and (G) were from the same trial and were photographed together. The same photographs of the control genotypes [wild-type and *olrn-1(ums9)*] are shown in (A), (E), and (G) to make interpretation of the figure easier.

(I) Brood sizes from animals of the indicated genotypes were quantified. Each data point is the average brood size from two animals. *$p < 0.05$ by one-way ANOVA for the indicated comparison. The data for each replicate are presented in Table S2.

Scale bars in (A), (C), (E), and (G) are 100 μm. See also Figure S3.

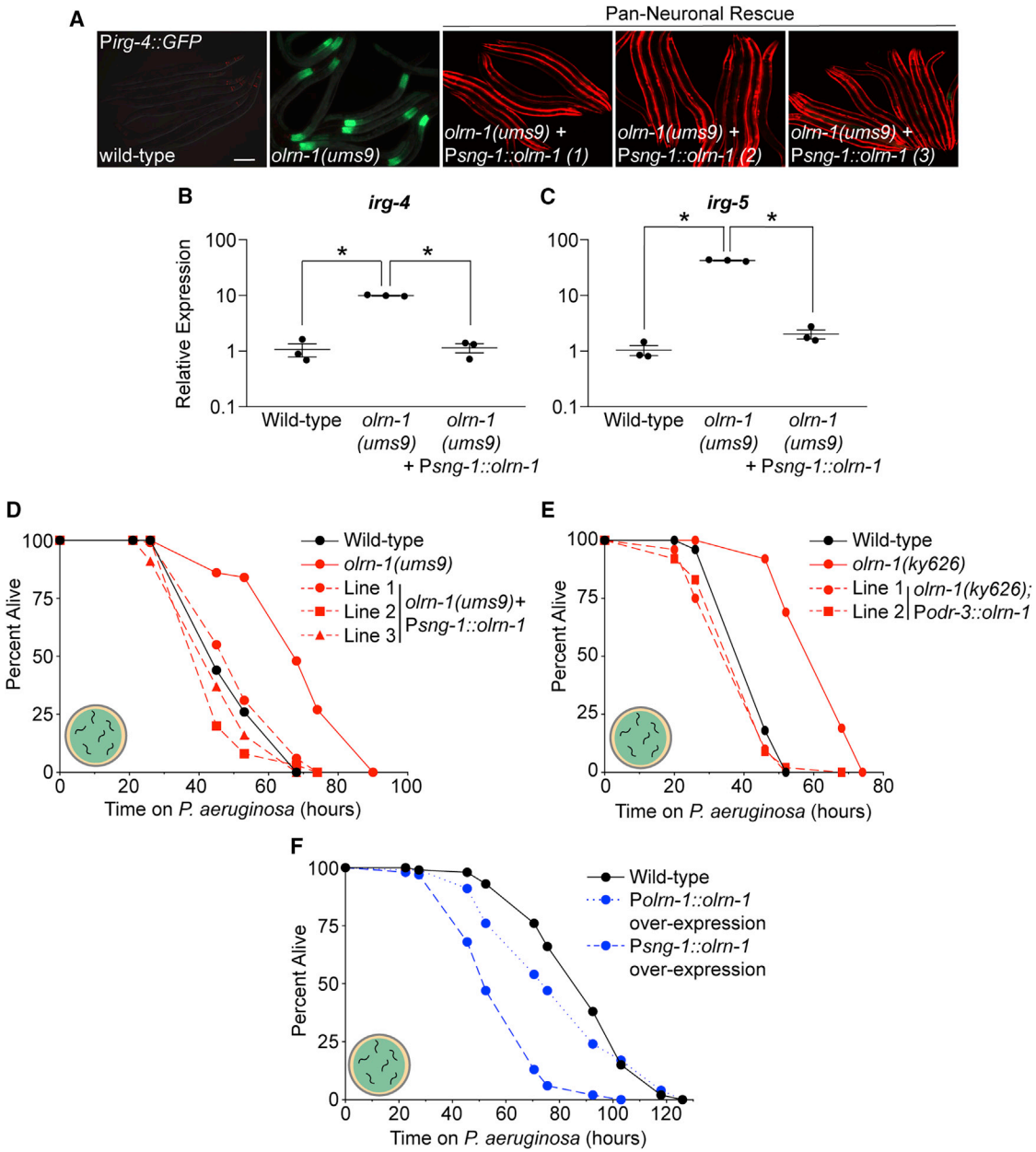

Figure 5. Expression of *olrn-1* in Chemosensory Neurons Is Sufficient to Regulate Innate Immunity in the Intestinal Epithelium

(A) Three independent lines of *olrn-1* under the control of a pan-neuronal promoter (*sng-1*) in the *olrn-1(ums9)* mutant, along with the *olrn-1(ums9)* mutant, are shown. P*myo-3::mCherry* expression indicates the presence of an extrachromosomal array that contains the P*sng-1::olrn-1* construct. Scale bar is 100 μm.

(B and C) qRT-PCR data show *irg-4* (B) and *irg-5* (C) expression in animals of the indicated genotypes. Data are the average of three independent replicates, each normalized to a control gene, with error bars representing SEM. Data are presented as the value relative to the average expression from all replicates of the indicated gene in wild-type animals. *p < 0.05 by one-way ANOVA for the indicated comparison.

(D–F) *C. elegans* pathogenesis assay conducted with a large lawn of *P. aeruginosa* and *C. elegans* of indicated genotypes at L4 is shown. Data are representative of three trials.

Sample sizes, mean lifespan, and p values for all trials are shown in Table S2. See also Figure S4.

genetic pathway that controls olfactory receptor development in AWC neurons. This work revealed that low *olrn-1* activity causes activation (de-repression) of the TIR-1/NSY-1/SEK-1/(PMK-1 or PMK-2) signaling cassette in AWC^{OFF} neurons (Bauer Huang et al., 2007; Troemel et al., 1997, 1999).

Given that the TIR-1/NSY-1/SEK-1/PMK-1 pathway is required both in neurons for the development of odorant receptors and in the intestine for innate immunity, we determined the tissues in which this signaling cassette is sufficient for the promotion of immune homeostasis by neuronal *olrn-1*. A P*ges-*

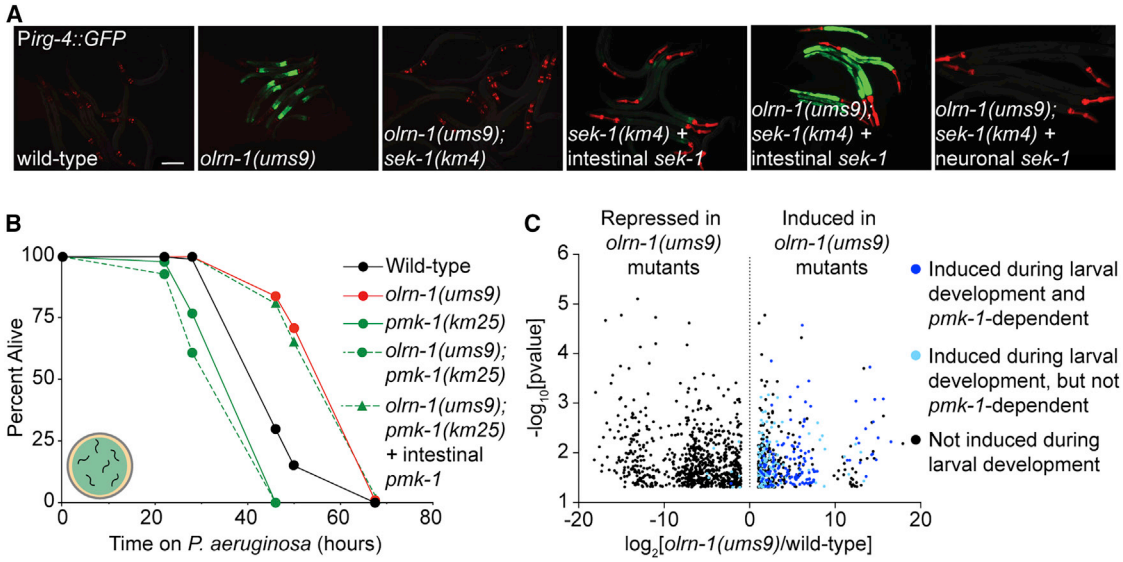

Figure 6. Immune Effectors Regulated by Neuronal *olrn-1* Are Dynamically Expressed during Nematode Development

(A) Representative images of animals with the indicated genotypes carrying an integrated P*irg-4::GFP* reporter. Red pharyngeal expression is the P*myo-2::mCherry* co-injection marker, which confirms the presence of the P*irg-4::GFP* transgene. Bright red pharyngeal expression in *C. elegans* with intestinal *sek-1* (P*ges-1::sek-1::GFP*) and neuronal *sek-1* (P*unc-119::sek-1::GFP*) is the P*myo-2:mStrawberry* co-injection marker. The presence of the P*irg-4::GFP* reporter was confirmed in these animals by P*myo-2::mCherry* expression in siblings that did not contain the indicated extrachromosomal arrays. Scale bar is 100 μm.

(B) *C. elegans* pathogenesis assay conducted with a large lawn of *P. aeruginosa* and *C. elegans* of indicated genotypes at L4 is shown. Data are representative of three trials. Sample sizes, mean lifespan, and p values for all trials are shown in Table S2. "Intestinal *pmk-1*" indicates that these animals have the P*vha-6::pmk-1* extrachromosomal array.

(C) Volcano plot of the mRNA-seq transcriptome profiling analysis shows all genes that were differentially expressed in *olrn-1(ums9)* mutants compared with wild-type animals (fold change > 2, $p < 0.05$), as described in Figure 2A. Highlighted in dark blue are the genes whose transcription are (1) dependent on the p38 MAPK *pmk-1* (from the overlap in Figure 2D) and (2) induced in wild-type animals at L1, L2, L3, or L4 compared with wild-type young adult animals. Highlighted in light blue are the genes that are induced in L1, L2, L3, or L4 wild-type nematodes compared with adult animals but whose transcription does not depend on p38 MAPK *pmk-1*.

Venn diagrams showing the overlap of genes that are induced at each larval stage compared with genes that are induced in *olrn-1(ums9)* mutants are shown Figure S5A. See also Figure S5.

1::sek-1::GFP construct, which directs *sek-1* expression in intestinal epithelial cells (Shivers et al., 2009), was introduced into the *olrn-1(ums9);sek-1(km4)* double mutant. Reconstitution of the p38 MAPKK *sek-1* in the intestine restored P*irg-4::GFP* expression in the *olrn-1(ums9);sek-1(km4)* double mutant (Figure 6A). To confirm our results with the P*ges-1::sek-1::GFP* construct using a different heterologous promoter, we introduced a P*vha-6::pmk-1* construct (Bolz et al., 2010) into the *olrn-1(ums9);pmk-1(km25)* double mutant. Like P*ges-1*, P*vha-6* directs gene expression specifically in intestinal epithelial cells (McGhee et al., 1990; Oka et al., 2001). Consistent with our observations with the P*ges-1::sek-1* construct (Figure 6A), intestinal expression of *pmk-1* was sufficient to restore the pathogen resistance phenotype of the *olrn-1(ums9)* mutant to the *olrn-1(ums9);pmk-1(km25)* double mutant (Figure 6B). However, expression of *sek-1* under the control of a neuronal-specific promoter (P*unc-119::sek-1*) (Shivers et al., 2009) in the *olrn-1(ums9);sek-1(km4)* double mutant did not restore constitutive activation of P*irg-4::GFP* in the *olrn-1(ums9)* mutant background (Figure 6A). Thus, the p38 MAPK PMK-1 pathway in intestinal epithelial cells, but not in neurons, is sufficient for the modulation of immune effector expression and resistance to *P. aeruginosa* infection by neuronal *olrn-1*.

The function of the innexin gene *nsy-5* and the claudin/calcium channel γ subunit gene *nsy-4* in promoting AWC neuron differentiation, as defined in genetic studies, is similar to that of *olrn-1* (Bauer Huang et al., 2007; Chuang et al., 2007; Vanhoven et al., 2006). Like *olrn-1* mutants, both *nsy-4(ky616)* and *nsy-5(ky634)* loss-of-function mutants have two AWC^{OFF} neurons, one of which never differentiates into an AWC^{ON} neuron (Bauer Huang et al., 2007). Interestingly, the immune effectors *irg-4* (Figure S4A) and *irg-5* (Figure S4B) are not constitutively induced in *nsy-4(ky616)* and *nsy-5(ky634)* loss-of-function mutants as they are in the *olrn-1* mutants. These data indicate that *olrn-1* has distinct roles in regulating immune effector expression in the intestine and promoting olfactory receptor development in AWC neurons.

Considering the role of *olrn-1* in controlling olfactory receptor development in AWC neurons, we asked whether *olrn-1*-dependent immune effectors are differentially expressed during larval development. We compared the RNA-seq transcriptome profiles of wild-type *C. elegans* at each larval stage and identified 707, 580, 717, 602, and 100 genes that were expressed at significantly higher levels in wild-type animals at the first larval stage (L1), the second larval stage (L2), the third larval stage (L3), the fourth larval stage (L4), and the young adult stage (YA)

compared with adult animals, respectively ($p < 0.05$, greater than 2-fold change). Genes that are expressed at higher levels in *olrn-1(ums9)* mutants are significantly enriched among the genes that are developmentally regulated in wild-type animals, including a significant number of the genes identified in Figure 2D that are targets of the *olrn-1*-p38 MAPK *pmk-1* signaling axis (Figures 6C and S5A). In particular, innate immune genes were enriched among the genes expressed higher in L3 animals compared with adults (p value for GO term enrichment 4.8×10^{-5}), as were genes induced during *P. aeruginosa* infection (hypergeometric p value 7.9e−10). In addition, we identified 100 genes that were expressed higher in young adult compared with adult animals, but neither *olrn-1*-regulated genes nor immune effectors in general were enriched in this dataset (Figure S5A). Using qRT-PCR, we confirmed that the *olrn-1*-dependent immune effectors *irg-4* (Figure S5B) and *irg-5* (Figure S5C) were expressed at higher levels in animals at L2/L3 compared with young adult animals. Low activity of OLRN-1 leads to de-repression of the p38 MAPK pathway in AWC neurons (Bauer Huang et al., 2007). Altogether, the data in this manuscript suggest that low levels of *olrn-1*, as recapitulated in multiple loss-of-function mutant alleles, de-repress the p38 MAPK PMK-1 pathway in intestine to promote pathogen resistance during *C. elegans* development.

DISCUSSION

This study demonstrates that innate immunity in *C. elegans* intestinal epithelial cells and the development of AWC neurons are linked by a single neuronal protein. Neuronal *olrn-1* functions cell autonomously in AWC neurons to ensure olfactory receptor expression and cell non-autonomously to suppress the p38 MAPK PMK-1 immune pathway in the intestine. We propose that low activity of neuronal OLRN-1 de-represses the p38 MAPK PMK-1 pathway to prime the immune response in the intestine to handle challenges from bacterial pathogens encountered during larval development.

The decision of a nematode to move toward nutritious bacteria and away from potential pathogens involves the integration of multiple inputs from different sensory neurons, including the chemosensation of pathogen-derived metabolites, recognizing attractive odors from food sources, monitoring oxygen availability, and sensing mechanical stimuli (Chang et al., 2011; Ha et al., 2010; Meisel et al., 2014; Pradel et al., 2007; Reddy et al., 2009; Zhang et al., 2005). AWC neurons detect attractive odorants and induce chemotaxis toward the stimuli (Bargmann et al., 1993; Troemel et al., 1997), but they do not control aversion responses to bacterial pathogens (Chang et al., 2011; Meisel et al., 2014; Zhang et al., 2005). As such, we did not observe defects in the ability of *olrn-1* mutants to avoid *P. aeruginosa*. It is intriguing that immune control in the intestine is linked to the development of neurons that promote chemotaxis. These data may speak to the importance of detecting attractive odorants from food sources for the ability of nematodes to develop in microbe-rich habitats.

We found that *olrn-1* is required to suppress the p38 MAPK PMK-1 pathway to prevent the deleterious effects of immune hyperactivation on *C. elegans* development and fecundity. These data support previous studies, which found that activation of the p38 MAPK PMK-1 pathway constitutes a source of physiological stress for *C. elegans*. For example, induction of immune effector expression during pathogen infection or by treatment with an immunostimulatory small molecule causes endoplasmic reticulum stress, which requires compensatory activation of the unfolded protein response (UPR) (Peterson et al., 2019; Richardson et al., 2010). In addition, we previously found that hyperactivation of immune defenses in the intestine by a gain-of-function mutation in the p38 MAPKKK *nsy-1* (*nsy-1(ums8)*) or by exogenous treatment with an immunostimulatory small molecule dramatically slowed nematode development in a manner dependent on the p38 MAPK PMK-1 pathway (Cheesman et al., 2016). Third, control of the p38 MAPK PMK-1 innate immune pathway by the C/EBP transcription factor CEBP-1 and the Tribbles kinase NIPI-3 is essential for development (Kim et al., 2016). Finally, other mechanisms that globally suppress p38 MAPK PMK-1 activity promote reproduction (Amrit et al., 2019). Altogether, these studies emphasize the physiological importance of mechanisms that control the activity of the p38 MAPK PMK-1 pathway and demonstrate that immune homeostasis is required for evolutionary fitness.

Two other neuronal mechanisms have been shown to suppress intestinal epithelial immune responses in *C. elegans*. Inhibition of dopamine signaling between CEP and ASG neurons suppresses immune activation in the nematode intestine (Cao and Aballay, 2016). In addition, the GPCR (G protein-coupled receptor) OCTR-1 functions in ASH and ASI neurons to negatively regulate a noncanonical branch of the UPR (Sun et al., 2011); downregulate protein synthesis (Liu et al., 2016); modulate the activity of multiple parallel stress response pathways, including *pmk-1*, *daf-16*, and *ced-1* (Cao et al., 2017; Sellegounder et al., 2018; Sun et al., 2011); and affect pathogen-avoidance behavior (Cao et al., 2017). A mutation in the neuropeptide gene *nlp-20* suppressed the immune effector induction and pathogen resistance phenotypes of *octr-1* loss-of-function mutants, suggesting that this neuropeptide may signal to the intestine to suppress innate immunity (Cao et al., 2017). We do not know how OLRN-1 and AWC neurons communicate with the intestine to regulate the p38 MAPK PMK-1 innate immune pathway. Because sensory neurons do not directly synapse with intestinal epithelial cells in *C. elegans*, we hypothesize that neurons communicate with the intestine via a relayed signal, such as a neuropeptide or another mechanism. In any case, immune control by CEP, ASG, ASH, and ASI neurons in *C. elegans* is not known to be integrated with the development of olfactory receptors in neurons, as we found is the case for the activity of OLRN-1 in AWC neurons.

Of note, OLRN-1 contains two putative transmembrane domains and is related to *Drosophila* Raw. In flies, Raw inhibits JNK MAPK signaling during development to promote dorsal closure of the fly embryo (Bauer Huang et al., 2007; Byars et al., 1999). The inhibitory effect of OLRN-1 and a related *Drosophila* protein on MAPK signaling suggests that a common mechanism may be employed by these proteins to suppress signal transduction.

The human intestine is densely innervated, and it is becoming increasingly appreciated that the enteric nervous system plays a key role in the maintenance of immune homeostasis (Tracey, 2010, 2014). However, disentangling the contribution of

individual sensory neurons in the regulation of intestinal inflammation has been challenging. In this regard, *C. elegans* has emerged as a useful system to define the wiring of neural-immune connections and to characterize the mechanisms that integrate immune control in the intestine with the physiology of the organism as a whole (Labed et al., 2018; Reddy et al., 2009; Styer et al., 2008). Here, we show that a single neuronal gene links regulation of innate immunity with the development of olfactory neuron receptors in *C. elegans*. Our findings suggest that integration of neuronal development programs with control of host immune defenses allows survival of animals that develop in microbe-rich environments.

STAR★METHODS

Detailed methods are provided in the online version of this paper and include the following:

- KEY RESOURCES TABLE
- LEAD CONTACT AND MATERIALS AVAILABILITY
- EXPERIMENTAL MODEL AND SUBJECT DETAILS
- METHOD DETAILS
  - Forward genetic screen
  - *C. elegans* Bacterial Infection and Other Assays
  - Generation of transgenic *C. elegans* strains
  - Gene expression analyses and bioinformatics
  - Immunoblot Analyses
  - Microscopy
- QUANTIFICATION AND STATISTICAL ANALYSIS
- DATA AND CODE AVAILABILITY

SUPPLEMENTAL INFORMATION

Supplemental Information can be found online at https://doi.org/10.1016/j.celrep.2020.03.042.

ACKNOWLEDGMENTS

The authors thank Cornelia Bargmann for providing nematode strains and acknowledge Cole Haynes, Robert Dowen, and Melanie Trombly for helpful discussions and critical reading of the manuscript. This research was supported by R01 AI130289 (to R.P.W.), an Innovator Award from the Kenneth Rainin Foundation (to R.P.W.), a Child Health Research Award from the Charles H. Hood Foundation (to R.P.W.), T32 AI095213 (to K.J.F.), and T32 AI132152 (to N.D.P.). Some strains were provided by the CGC, which is funded by NIH Office of Research Infrastructure Programs (P40 OD010440).

AUTHOR CONTRIBUTIONS

Conceptualization, R.P.W.; Investigation, K.J.F., H.K.C., N.D.P., S.M.A., and R.P.W.; Formal Analysis, K.J.F., H.K.C., N.D.P., and R.P.W.; Validation, K.J.F., H.K.C., N.D.P., and R.P.W.; Software, P.L.; Writing – Original Draft, R.P.W.; Writing – Review & Editing, R.P.W. and K.J.F.; Project Administration, R.P.W.; Funding Acquisition, R.P.W.

DECLARATION OF INTERESTS

R.P.W. has submitted a patent application related to this work (U.S. patent application, 16/069,399, filed July 11, 2018). The authors declare no other potential competing interests.

Received: October 8, 2019
Revised: January 15, 2020
Accepted: March 13, 2020
Published: April 7, 2020

REFERENCES

Amrit, F.R.G., Naim, N., Ratnappan, R., Loose, J., Mason, C., Steenberge, L., McClendon, B.T., Wang, G., Driscoll, M., Yanowitz, J.L., and Ghazi, A. (2019). The longevity-promoting factor, TCER-1, widely represses stress resistance and innate immunity. Nat. Commun. *10*, 3042.

Anderson, S.M., Cheesman, H.K., Peterson, N.D., Salisbury, J.E., Soukas, A.A., and Pukkila-Worley, R. (2019). The fatty acid oleate is required for innate immune activation and pathogen defense in *Caenorhabditis elegans*. PLoS Pathog. *15*, e1007893.

Bargmann, C.I., Hartwieg, E., and Horvitz, H.R. (1993). Odorant-selective genes and neurons mediate olfaction in *C. elegans*. Cell *74*, 515–527.

Bauer Huang, S.L., Saheki, Y., VanHoven, M.K., Torayama, I., Ishihara, T., Katsura, I., van der Linden, A., Sengupta, P., and Bargmann, C.I. (2007). Left-right olfactory asymmetry results from antagonistic functions of voltage-activated calcium channels and the Raw repeat protein OLRN-1 in *C. elegans*. Neural Dev. *2*, 24.

Bolger, A.M., Lohse, M., and Usadel, B. (2014). Trimmomatic: a flexible trimmer for Illumina sequence data. Bioinformatics *30*, 2114–2120.

Bolz, D.D., Tenor, J.L., and Aballay, A. (2010). A conserved PMK-1/p38 MAPK is required in *Caenorhabditis elegans* tissue-specific immune response to *Yersinia pestis* infection. J. Biol. Chem. *285*, 10832–10840.

Bond, M.R., Ghosh, S.K., Wang, P., and Hanover, J.A. (2014). Conserved nutrient sensor O-GlcNAc transferase is integral to *C. elegans* pathogen-specific immunity. PLoS ONE *9*, e113231.

Brenner, S. (1974). The genetics of *Caenorhabditis elegans*. Genetics *77*, 71–94.

Byars, C.L., Bates, K.L., and Letsou, A. (1999). The dorsal-open group gene raw is required for restricted DJNK signaling during closure. Development *126*, 4913–4923.

Cao, X., and Aballay, A. (2016). Neural Inhibition of Dopaminergic Signaling Enhances Immunity in a Cell-Non-autonomous Manner. Curr. Biol. *26*, 2329–2334.

Cao, X., Kajino-Sakamoto, R., Doss, A., and Aballay, A. (2017). Distinct Roles of Sensory Neurons in Mediating Pathogen Avoidance and Neuropeptide-Dependent Immune Regulation. Cell Rep. *21*, 1442–1451.

Chang, H.C., Paek, J., and Kim, D.H. (2011). Natural polymorphisms in *C. elegans* HECW-1 E3 ligase affect pathogen avoidance behaviour. Nature *480*, 525–529.

Cheesman, H.K., Feinbaum, R.L., Thekkiniath, J., Dowen, R.H., Conery, A.L., and Pukkila-Worley, R. (2016). Aberrant Activation of p38 MAP Kinase-Dependent Innate Immune Responses Is Toxic to *Caenorhabditis elegans*. G3 (Bethesda) *6*, 541–549.

Chuang, C.F., and Bargmann, C.I. (2005). A Toll-interleukin 1 repeat protein at the synapse specifies asymmetric odorant receptor expression via ASK1 MAPKKK signaling. Genes Dev. *19*, 270–281.

Chuang, C.F., Vanhoven, M.K., Fetter, R.D., Verselis, V.K., and Bargmann, C.I. (2007). An innexin-dependent cell network establishes left-right neuronal asymmetry in *C. elegans*. Cell *129*, 787–799.

Estes, K.A., Dunbar, T.L., Powell, J.R., Ausubel, F.M., and Troemel, E.R. (2010). bZIP transcription factor *zip-2* mediates an early response to *Pseudomonas aeruginosa* infection in *Caenorhabditis elegans*. Proc. Natl. Acad. Sci. USA *107*, 2153–2158.

Ewels, P., Magnusson, M., Lundin, S., and Käller, M. (2016). MultiQC: summarize analysis results for multiple tools and samples in a single report. Bioinformatics *32*, 3047–3048.

Foster, K.J., McEwan, D.L., and Pukkila-Worley, R. (2020). Measurements of Innate Immune Function in *C. elegans*. In Aging: Methods and Protocols, S.P. Curran, ed. (Springer Nature (in press)).

Gibson, D.G., Young, L., Chuang, R.Y., Venter, J.C., Hutchison, C.A., 3rd, and Smith, H.O. (2009). Enzymatic assembly of DNA molecules up to several hundred kilobases. Nat. Methods *6*, 343–345.

Ha, H.I., Hendricks, M., Shen, Y., Gabel, C.V., Fang-Yen, C., Qin, Y., Colón-Ramos, D., Shen, K., Samuel, A.D., and Zhang, Y. (2010). Functional organization of a neural network for aversive olfactory learning in *Caenorhabditis elegans*. Neuron *68*, 1173–1186.

Haenni, S., Ji, Z., Hoque, M., Rust, N., Sharpe, H., Eberhard, R., Browne, C., Hengartner, M.O., Mellor, J., Tian, B., and Furger, A. (2012). Analysis of *C. elegans* intestinal gene expression and polyadenylation by fluorescence-activated nuclei sorting and 3′-end-seq. Nucleic Acids Res. *40*, 6304–6318.

Han, S.K., Lee, D., Lee, H., Kim, D., Son, H.G., Yang, J.S., Lee, S.V., and Kim, S. (2016). OASIS 2: online application for survival analysis 2 with features for the analysis of maximal lifespan and healthspan in aging research. Oncotarget *7*, 56147–56152.

Kim, D.H., and Ewbank, J.J. (2018). Signaling in the innate immune response. WormBook *2018*, 1–35.

Kim, D.H., Feinbaum, R., Alloing, G., Emerson, F.E., Garsin, D.A., Inoue, H., Tanaka-Hino, M., Hisamoto, N., Matsumoto, K., Tan, M.W., and Ausubel, F.M. (2002). A conserved p38 MAP kinase pathway in *Caenorhabditis elegans* innate immunity. Science *297*, 623–626.

Kim, D., Langmead, B., and Salzberg, S.L. (2015). HISAT: a fast spliced aligner with low memory requirements. Nat. Methods *12*, 357–360.

Kim, K.W., Thakur, N., Piggott, C.A., Omi, S., Polanowska, J., Jin, Y., and Pujol, N. (2016). Coordinated inhibition of C/EBP by Tribbles in multiple tissues is essential for *Caenorhabditis elegans* development. BMC Biol. *14*, 104.

Labed, S.A., Wani, K.A., Jagadeesan, S., Hakkim, A., Najibi, M., and Irazoqui, J.E. (2018). Intestinal Epithelial Wnt Signaling Mediates Acetylcholine-Triggered Host Defense against Infection. Immunity *48*, 963–978.

Li, H. (2011). A statistical framework for SNP calling, mutation discovery, association mapping and population genetical parameter estimation from sequencing data. Bioinformatics *27*, 2987–2993.

Li, H. (2018). Minimap2: pairwise alignment for nucleotide sequences. Bioinformatics *34*, 3094–3100.

Li, H., Handsaker, B., Wysoker, A., Fennell, T., Ruan, J., Homer, N., Marth, G., Abecasis, G., and Durbin, R.; 1000 Genome Project Data Processing Subgroup (2009). The Sequence Alignment/Map format and SAMtools. Bioinformatics *25*, 2078–2079.

Liberati, N.T., Fitzgerald, K.A., Kim, D.H., Feinbaum, R., Golenbock, D.T., and Ausubel, F.M. (2004). Requirement for a conserved Toll/interleukin-1 resistance domain protein in the *Caenorhabditis elegans* immune response. Proc. Natl. Acad. Sci. USA *101*, 6593–6598.

Liu, Y., Sellegounder, D., and Sun, J. (2016). Neuronal GPCR OCTR-1 regulates innate immunity by controlling protein synthesis in *Caenorhabditis elegans*. Sci. Rep. *6*, 36832.

McGhee, J.D., Birchall, J.C., Chung, M.A., Cottrell, D.A., Edgar, L.G., Svendsen, P.C., and Ferrari, D.C. (1990). Production of null mutants in the major intestinal esterase gene (*ges-1*) of the nematode *Caenorhabditis elegans*. Genetics *125*, 505–514.

Meisel, J.D., Panda, O., Mahanti, P., Schroeder, F.C., and Kim, D.H. (2014). Chemosensation of bacterial secondary metabolites modulates neuroendocrine signaling and behavior of *C. elegans*. Cell *159*, 267–280.

Miller, E.V., Grandi, L.N., Giannini, J.A., Robinson, J.D., and Powell, J.R. (2015). The Conserved G-Protein Coupled Receptor FSHR-1 Regulates Protective Host Responses to Infection and Oxidative Stress. PLoS ONE *10*, e0137403.

Minevich, G., Park, D.S., Blankenberg, D., Poole, R.J., and Hobert, O. (2012). CloudMap: a cloud-based pipeline for analysis of mutant genome sequences. Genetics *192*, 1249–1269.

Nandakumar, M., and Tan, M.W. (2008). Gamma-linolenic and stearidonic acids are required for basal immunity in *Caenorhabditis elegans* through their effects on p38 MAP kinase activity. PLoS Genet. *4*, e1000273.

Oka, T., Toyomura, T., Honjo, K., Wada, Y., and Futai, M. (2001). Four subunit a isoforms of *Caenorhabditis elegans* vacuolar H+-ATPase. Cell-specific expression during development. J. Biol. Chem. *276*, 33079–33085.

Pagano, D.J., Kingston, E.R., and Kim, D.H. (2015). Tissue expression pattern of PMK-2 p38 MAPK is established by the miR-58 family in *C. elegans*. PLoS Genet. *11*, e1004997.

Pertea, M., Pertea, G.M., Antonescu, C.M., Chang, T.C., Mendell, J.T., and Salzberg, S.L. (2015). StringTie enables improved reconstruction of a transcriptome from RNA-seq reads. Nat. Biotechnol. *33*, 290–295.

Pertea, M., Kim, D., Pertea, G.M., Leek, J.T., and Salzberg, S.L. (2016). Transcript-level expression analysis of RNA-seq experiments with HISAT, StringTie and Ballgown. Nat. Protoc. *11*, 1650–1667.

Peterson, N.D., Cheesman, H.K., Liu, P., Anderson, S.M., Foster, K.J., Chhaya, R., Perrat, P., Thekkiniath, J., Yang, Q., Haynes, C.M., and Pukkila-Worley, R. (2019). The nuclear hormone receptor NHR-86 controls anti-pathogen responses in *C. elegans*. PLoS Genet. *15*, e1007935.

Pfaffl, M.W. (2001). A new mathematical model for relative quantification in real-time RT-PCR. Nucleic Acids Res. *29*, e45.

Powell, J.R., Kim, D.H., and Ausubel, F.M. (2009). The G protein-coupled receptor FSHR-1 is required for the *Caenorhabditis elegans* innate immune response. Proc. Natl. Acad. Sci. USA *106*, 2782–2787.

Pradel, E., Zhang, Y., Pujol, N., Matsuyama, T., Bargmann, C.I., and Ewbank, J.J. (2007). Detection and avoidance of a natural product from the pathogenic bacterium *Serratia marcescens* by *Caenorhabditis elegans*. Proc. Natl. Acad. Sci. USA *104*, 2295–2300.

Pukkila-Worley, R. (2016). Surveillance Immunity: An Emerging Paradigm of Innate Defense Activation in *Caenorhabditis elegans*. PLoS Pathog. *12*, e1005795.

Pukkila-Worley, R., Feinbaum, R., Kirienko, N.V., Larkins-Ford, J., Conery, A.L., and Ausubel, F.M. (2012). Stimulation of host immune defenses by a small molecule protects *C. elegans* from bacterial infection. PLoS Genet. *8*, e1002733.

Pukkila-Worley, R., Feinbaum, R.L., McEwan, D.L., Conery, A.L., and Ausubel, F.M. (2014). The evolutionarily conserved mediator subunit MDT-15/MED15 links protective innate immune responses and xenobiotic detoxification. PLoS Pathog. *10*, e1004143.

Rahme, L.G., Stevens, E.J., Wolfort, S.F., Shao, J., Tompkins, R.G., and Ausubel, F.M. (1995). Common virulence factors for bacterial pathogenicity in plants and animals. Science *268*, 1899–1902.

Reddy, K.C., Andersen, E.C., Kruglyak, L., and Kim, D.H. (2009). A polymorphism in *npr-1* is a behavioral determinant of pathogen susceptibility in *C. elegans*. Science *323*, 382–384.

Reddy, K.C., Dunbar, T.L., Nargund, A.M., Haynes, C.M., and Troemel, E.R. (2016). The *C. elegans* CCAAT-Enhancer-Binding Protein Gamma Is Required for Surveillance Immunity. Cell Rep. *14*, 1581–1589.

Richardson, C.E., Kooistra, T., and Kim, D.H. (2010). An essential role for XBP-1 in host protection against immune activation in *C. elegans*. Nature *463*, 1092–1095.

Roach, N.P., Sadowski, N., Alessi, A.F., Timp, W., Taylor, J., and Kim, J.K. (2019). The full-length transcriptome of *C. elegans* using direct RNA sequencing. bioRxiv. https://doi.org/10.1101/598763.

Roayaie, K., Crump, J.G., Sagasti, A., and Bargmann, C.I. (1998). The G alpha protein ODR-3 mediates olfactory and nociceptive function and controls cilium morphogenesis in *C. elegans* olfactory neurons. Neuron *20*, 55–67.

Sellegounder, D., Yuan, C.H., Wibisono, P., Liu, Y., and Sun, J. (2018). Octopaminergic Signaling Mediates Neural Regulation of Innate Immunity in *Caenorhabditis elegans*. MBio *9*, e01645-18.

Shapira, M., Hamlin, B.J., Rong, J., Chen, K., Ronen, M., and Tan, M.W. (2006). A conserved role for a GATA transcription factor in regulating epithelial innate immune responses. Proc. Natl. Acad. Sci. USA *103*, 14086–14091.

Shivers, R.P., Kooistra, T., Chu, S.W., Pagano, D.J., and Kim, D.H. (2009). Tissue-specific activities of an immune signaling module regulate physiological responses to pathogenic and nutritional bacteria in *C. elegans*. Cell Host Microbe *6*, 321–330.

Shivers, R.P., Pagano, D.J., Kooistra, T., Richardson, C.E., Reddy, K.C., Whitney, J.K., Kamanzi, O., Matsumoto, K., Hisamoto, N., and Kim, D.H. (2010). Phosphorylation of the conserved transcription factor ATF-7 by PMK-1 p38 MAPK regulates innate immunity in *Caenorhabditis elegans*. PLoS Genet. *6*, e1000892.

Singh, J., and Aballay, A. (2019). Microbial Colonization Activates an Immune Fight-and-Flight Response via Neuroendocrine Signaling. Dev. Cell *49*, 89–99.

Styer, K.L., Singh, V., Macosko, E., Steele, S.E., Bargmann, C.I., and Aballay, A. (2008). Innate immunity in *Caenorhabditis elegans* is regulated by neurons expressing NPR-1/GPCR. Science *322*, 460–464.

Sun, J., Singh, V., Kajino-Sakamoto, R., and Aballay, A. (2011). Neuronal GPCR controls innate immunity by regulating noncanonical unfolded protein response genes. Science *332*, 729–732.

Tan, M.W., Mahajan-Miklos, S., and Ausubel, F.M. (1999). Killing of *Caenorhabditis elegans* by *Pseudomonas aeruginosa* used to model mammalian bacterial pathogenesis. Proc. Natl. Acad. Sci. USA *96*, 715–720.

Torayama, I., Ishihara, T., and Katsura, I. (2007). *Caenorhabditis elegans* integrates the signals of butanone and food to enhance chemotaxis to butanone. J. Neurosci. *27*, 741–750.

Tracey, K.J. (2010). Understanding immunity requires more than immunology. Nat. Immunol. *11*, 561–564.

Tracey, K.J. (2014). Approaching the next revolution? Evolutionary integration of neural and immune pathogen sensing and response. Cold Spring Harb. Perspect. Biol. *7*, a016360.

Troemel, E.R., Kimmel, B.E., and Bargmann, C.I. (1997). Reprogramming chemotaxis responses: sensory neurons define olfactory preferences in *C. elegans*. Cell *91*, 161–169.

Troemel, E.R., Sagasti, A., and Bargmann, C.I. (1999). Lateral signaling mediated by axon contact and calcium entry regulates asymmetric odorant receptor expression in *C. elegans*. Cell *99*, 387–398.

Troemel, E.R., Chu, S.W., Reinke, V., Lee, S.S., Ausubel, F.M., and Kim, D.H. (2006). p38 MAPK regulates expression of immune response genes and contributes to longevity in *C. elegans*. PLoS Genet. *2*, e183.

Vanhoven, M.K., Bauer Huang, S.L., Albin, S.D., and Bargmann, C.I. (2006). The claudin superfamily protein *nsy-4* biases lateral signaling to generate left-right asymmetry in *C. elegans* olfactory neurons. Neuron *51*, 291–302.

Wes, P.D., and Bargmann, C.I. (2001). *C. elegans* odour discrimination requires asymmetric diversity in olfactory neurons. Nature *410*, 698–701.

Wingett, S.W., and Andrews, S. (2018). FastQ Screen: A tool for multi-genome mapping and quality control. F1000Res. *7*, 1338.

Zhang, Y., Lu, H., and Bargmann, C.I. (2005). Pathogenic bacteria induce aversive olfactory learning in *Caenorhabditis elegans*. Nature *438*, 179–184.

STAR★METHODS

KEY RESOURCES TABLE

REAGENT or RESOURCE	SOURCE	IDENTIFIER
Antibodies		
Total PMK-1 Antibody	Peterson et al., 2019	N/A
Anti-p38 MAPK, phospho (Thr180 / Tyr182) Antibody, Unconjugated	Cell Signaling Technology	Cat# 9211
		RRID:AB_331641
		Lot# 25
Monoclonal Anti-alpha-Tubulin antibody produced in mouse	Sigma-Aldrich	Cat# T5168
		RRID:AB_477579
		Lot# 038M4813V
Anti-rabbit IgG, HRP-linked Antibody	Cell Signaling Technology	Cat# 7074
		RRID:AB_2099233
		Lot# 28
Goat Anti-Mouse IgG - H&L Polyclonal Antibody, HRP Conjugated	Abcam	Cat# ab6789
		RRID:AB_955439
		Lot# GR3216437-2
Bacterial and Virus Strains		
Escherichia coli OP50	Brenner, 1974	RRID:WB-STRAIN:OP50
Pseudomonas aeruginosa (UCBPP-PA14)	Rahme et al., 1995	RRID:WB-STRAIN:PA14
Chemicals, Peptides, and Recombinant Proteins		
5-Fluoro-2′-deoxyuridine	Sigma-Aldrich	Cat# CAF0503
(–) Tetramisole hydrochloride	Sigma-Aldrich	Cat# L9756-10G
EcoRI Restriction Enzyme	New England BioLabs	Cat# R0101
Q5 High-Fidelity DNA Polymerase	New England BioLabs	Cat# M0491S
Isopropyl-β-D-thiogalactoside	Research Products International	CAT# L56000
Trizol	Thermo Fisher Scientific	Cat# 15596018
Proteinase K	New England BioLabs	Cat# P8107S
Phenol:chloroform:isoamyl alcohol	Thermo Fisher	Cat# 15593031
Critical Commercial Assays		
Gibson Assembly Cloning Kit	New England BioLabs	Cat# E5510S
iScript gDNA Clear cDNA Synthesis Kit	Bio-Rad	Cat# 172-5034
iTaq Universal SYBR Green Supermix	Bio-Rad	Cat# 1725120
Deposited Data		
Raw and analyzed mRNA-Seq data	This study	GEO:GSE130959
Experimental Models: Organisms/Strains		
C. elegans: Strain: N2 (Bristol)	*Caenorhabditis* Genetics Center	WB Cat# WBStrain00000001; RRID:WB-STRAIN:WBStrain00000001
C. elegans: Strain: KU25 *pmk-1(km25)*	Kim et al., 2002	WB Cat# WBStrain00024040; RRID:WB-STRAIN:WBStrain00024040
C. elegans: Strain: AU306 *agIs44 [Pirg-4::GFP::unc-54-3′UTR; Pmyo-2::mCherry]*	Pukkila-Worley et al., 2014	N/A
C. elegans: Strain: AY101 *acIs101 [PDB09.1(Pirg-5::GFP); pRF4(rol-6(su1006))]*	Bolz et al., 2010	WB Cat# WBStrain00000322; RRID:WB-STRAIN:WBStrain00000322
C. elegans: Strain: RPW40 *olrn-1(ums9); agIs44[Pirg-4::GFP::unc-54-3′UTR; Pmyo-2::mCherry]*	This study	N/A
C. elegans: Strain: RPW31 *olrn-1(ums11); agIs44[Pirg-4::GFP::unc-54-3′UTR; Pmyo-2::mCherry]*	This study	N/A

(*Continued on next page*)

Continued

REAGENT or RESOURCE	SOURCE	IDENTIFIER
C. elegans: Strain: RPW222 *olrn-1(ky626); agIs44[Pirg-4::GFP::unc-54-3′UTR; Pmyo-2::mCherry]*	This study	N/A
C. elegans: Strain: RPW211 *olrn-1(ums9); acIs101 [PDB09.1(Pirg-5::GFP); pRF4(rol-6(su1006))]*	This study	N/A
C. elegans: Strain: ZD101 *tir-1(qd4)*	Shivers et al., 2009	WB Cat# WBStrain00040806; RRID:WB-STRAIN:WBStrain00040806
C. elegans: Strain: RPW43 *nsy-1(ums8); agIs44[Pirg-4::GFP::unc-54-3′UTR; Pmyo-2::mCherry]*	Cheesman et al., 2016	WormBase ID: WBVar02145386
C. elegans: Strain: RPW 129 *olrn-1(ums9);pmk-1(km25)*	This study	N/A
C. elegans: Strain: RPW189 *olrn-1(ums9);tir-1(qd4); agIs44[Pirg-4::GFP::unc-54-3′UTR; Pmyo-2::mCherry]*	This study	N/A
C. elegans: Strain: RPW131 *orln-1(ums9); agIs44[Pirg-4::GFP::unc-54-3′UTR; Pmyo-2::mCherry]; umsEx4 [Porln-1::orln-1;3′UTRorln-1; Pmyo-3::mCherry]*	This study	N/A
C. elegans: Strain: RPW133 *orln-1(ums9); agIs44[Pirg-4::GFP::unc-54-3′UTR; Pmyo-2::mCherry];umsEx6 [Porln-1::orln-1;3′UTRorln-1; Pmyo-3::mCherry]*	This study	N/A
C. elegans: Strain: RPW134 *orln-1(ums9); agIs44[Pirg-4::GFP::unc-54-3′UTR; Pmyo-2::mCherry];umsEx7 [Porln-1::orln-1;3′UTRorln-1; Pmyo-3::mCherry]*	This study	N/A
C. elegans: Strain: RPW159 *orln-1(ums9); agIs44[Pirg-4::GFP::unc-54-3′UTR; Pmyo-2::mCherry];umsEx20 [Psng-1::orln-1;3′UTRorln-1; Pmyo-3::mCherry]*	This study	N/A
C. elegans: Strain: RPW160 *orln-1(ums9); agIs44[Pirg-4::GFP::unc-54-3′UTR; Pmyo-2::mCherry];umsEx21 [Psng-1::orln-1;3′UTRorln-1; Pmyo-3::mCherry]*	This study	N/A
C. elegans: Strain: RPW162 *orln-1(ums9); agIs44[Pirg-4::GFP::unc-54-3′UTR; Pmyo-2::mCherry];umsEx23 [Psng-1::orln-1;3′UTRorln-1; Pmyo-3::mCherry]*	This study	N/A
C. elegans: Strain: CX7517 *olrn-1(ky626); kyEx914 [Podr-3::olrn-1;Podr-1::mCherry;coel::GFP]*	Bauer Huang et al., 2007	Laboratory of Cornelia Bargmann: Strain ID CX7517
C. elegans: Strain: CX7521 *olrn-1(ky626); kyEx918 [Podr-3::olrn-1;Podr-1::mCherry;coel::GFP]*	Bauer Huang et al., 2007	Laboratory of Cornelia Bargmann: Strain ID CX7521
C. elegans: Strain: *olrn-1(ky626)*	Bauer Huang et al., 2007	WormBase ID: WBVar00088455
C. elegans: Strain: RPW207 *agIs44[Pirg-4::GFP::unc-54-3′UTR; Pmyo-2::mCherry]; umsEx4 (Porln-1::orln-1;3′UTRorln-1; Pmyo-3::mCherry)*	This study	N/A
C. elegans: Strain: RPW209 *agIs44[Pirg-4::GFP::unc-54-3′UTR; Pmyo-2::mCherry]; umsEx21 (Psng-1::orln-1;3′UTRorln-1; Pmyo-3::mCherry)*	This study	N/A
C. elegans: Strain: RPW216 *atf-7(qd22 qd130); agIs219[T24B8.5::GFP]; olrn-1(ums9)*	This study	N/A
C. elegans: Strain: RPW218 *orln-1 (ums9); pmk-1(km25); acEx102 [vha-6p::pmk-1::GFP + rol-6(su1006)]*	This study	N/A
C. elegans: Strain: AY102 *pmk-1(km25); acEx102 [vha-6p::pmk-1::GFP + rol-6(su1006)]*	Bolz et al., 2010	WB Cat# WBStrain00000323; RRID:WB-STRAIN:WBStrain000003233

(*Continued on next page*)

Continued

REAGENT or RESOURCE	SOURCE	IDENTIFIER
C. elegans: Strain: ZD193 *sek-1(km4);qdEx4 [*Pges-1*::*sek-1*(cDNA)::GFP::*unc-54-3′ *UTR* + myo-2p*::mStrawberry::*unc-54-3′ UTR]*	Shivers et al., 2009	WB Cat# WBStrain00040807; RRID:WB-STRAIN:WBStrain00040807
C. elegans: Strain: ZD202 *sek-1(km4);qdEx8 [*Punc-119*::*sek-1*(cDNA)::GFP::*unc-54-3′ *UTR* + myo-2p*::mStrawberry::*unc-54-3′ UTR]*	Shivers et al., 2009	WB Cat# WBStrain00040808; RRID:WB-STRAIN:WBStrain00040808
C. elegans: Strain: RPW220 *olrn-1(ums9); sek-1(km4); agIs44*	This study	N/A
C. elegans: Strain: RPW227 *olrn-1(ums9); sek-1(km4); agIs44; qdEx4*	This study	N/A
C. elegans: Strain: RPW224 *olrn-1(ums9); sek-1(km4); agIs44; qdEx8*	This study	N/A
C. elegans: Strain: CX5757 *kyIs140 I; nsy-4(ky616) IV.*	*Caenorhabditis* Genetics Center	WB Cat# WBStrain00005274; RRID:WB-STRAIN:WBStrain00005274
C. elegans: Strain: (CX6161) *inx-19(ky634) I.*	*Caenorhabditis* Genetics Center	WB Cat# WBStrain00005278; RRID:WB-STRAIN:WBStrain00005278
Oligonucleotides		
olrn-1 Rescue PCR FWD primer: CAGAACCAGATTCTCGGAATGA	IDT	N/A
olrn-1 Rescue PCR REV primer: AGAGGAAGAGAGACAGGATGAA	IDT	N/A
Gibson Assembly Primer for *Psng-1*::*olrn-1b* construct: CCCCCCCTCGAGGTCGACGGTATCGATAAGCTTGATATCGt tgagcagcgactaacaaaa	IDT	N/A
Gibson Assembly Primer for *Psng-1*::*olrn-1b* construct: ACCTGACACTAATTTCTCTTGGCGCTGAACATCTAGTCAT gctaaaataaaagaaatata	IDT	N/A
Gibson Assembly Primer for P*sng-1*::*olrn-1b* construct: atgactagatgttcagcgcc	IDT	N/A
Gibson Assembly Primer for P*sng-1*::*olrn-1b* construct: GGCGGCCGCTCTAGAACTAGTGGATCCCCCGGGCTGCAG Gtttcatatatcttatgccgt	IDT	N/A
Recombinant DNA		
Plasmid: pBluescript SK(-)	Addgene	N/A
Software and Algorithms		
GraphPad Prism 8	Graphpad	https://www.graphpad.com/scientific-software/prism/
OASIS 2	Han et al., 2016	https://sbi.postech.ac.kr/oasis2/
Adobe Creative Cloud	Adobe	https://www.adobe.com/creativecloud.html
ApE: A plasmid Editor	M. Wayne Davis	http://jorgensen.biology.utah.edu/wayned/ape/
Microsoft Excel	Microsoft	https://office.live.com/start/Excel.aspx
FastQC (Version 0.11.8)	Wingett and Andrews, 2018	https://www.bioinformatics.babraham.ac.uk/projects/download.html
Multiqc (Version 1.7)	Ewels et al., 2016	https://github.com/ewels/MultiQC
Trimmomatic (Version 0.36)	Bolger et al., 2014	http://www.usadellab.org/cms/?page=trimmomatic
HISAT2 (Version 2.1.0)	Kim et al., 2015; Pertea et al., 2016	https://ccb.jhu.edu/software/hisat2/index.shtml
Samtools (Version 1.3.1)	Li, 2011; Li et al., 2009	https://sourceforge.net/projects/samtools/files/samtools/1.3.1/
Stringtie (Version 1.3.4)	Pertea et al., 2015, 2016	https://ccb.jhu.edu/software/stringtie/

(*Continued on next page*)

Continued

REAGENT or RESOURCE	SOURCE	IDENTIFIER
Ballgown (Version 3.8)	Pertea et al., 2016	https://www.bioconductor.org/packages/release/bioc/html/ballgown.html
R Console (Version 3.5)	The R Foundation	https://www.r-project.org/

LEAD CONTACT AND MATERIALS AVAILABILITY

All requests for reagents and further information regarding the protocols in this manuscript may be directed to the Lead Contact, Read Pukkila-Worley (Read.Pukkila-Worley@umassmed.edu). All unique/stable reagents generated in this study are available from the Lead Contact with a completed Materials Transfer Agreement.

EXPERIMENTAL MODEL AND SUBJECT DETAILS

C. elegans strains were maintained on standard nematode growth media (NGM) plates with *E. coli* OP50 as a food source, as described (Brenner, 1974). Mutant *C. elegans* and transgenic strains used in this study are presented in the Key Resources Table. *Pseudomonas aeruginosa* strain PA14 was used for all studies (Rahme et al., 1995).

METHOD DETAILS

Forward genetic screen

Ethyl methanesulfonate (EMS) mutagenesis was performed on strain *agIs44* as previously described (Cheesman et al., 2016). Synchronized F2 progeny representing approximately 40,000 haploid genomes were screened for animals that constitutively express *agIs44* GFP fluorescence. Three alleles were identified (*ums9, ums10* and *ums11*). To identify the causative mutations, pooled genomes from 52 recombinants for *ums9* and 3 recombinants for *ums11* following a 2X outcross to N2 were sequenced along with the *agIs44* parent strain. All recombinants constitutively expressed *agIs44* GFP. Homozygous variants from WS220 (ce10) *C. elegans* reference genome that were present in the 2X outcrossed samples, but not in *agIs44*, were identified using Cloud Map (Minevich et al., 2012). We were unable to identify the causative mutation in *ums10*.

C. elegans Bacterial Infection and Other Assays

"Slow killing" *P. aeruginosa* infection experiments were performed as previously described (Foster et al., 2020; Tan et al., 1999). The wild-type control for these assays is *agIs44*. In brief, a single colony of *P. aeruginosa* PA14 was inoculated into 5 mL of Luria-Bertani (LB) medium, and allowed to incubate at 37° for 15 hr. 10 μL of this culture was spread onto 35-mm tissue culture plates containing 4 mL of slow kill agar (0.35% peptone, 0.3% sodium chloride, 1.7% agar, 5 μg/ml cholesterol, 25 mM potassium phosphate, 1 mM magnesium sulfate, 1 mM calcium chloride). Plates were incubated for 24 hours at 37°C, and approximately 24 hours at 25°C. Approximately one hour before the start of the assay, 0.1 mg/ml 5-fluorodeoxyuridine (FUDR) was added to the medium to prevent progeny from hatching. For all pathogenesis assays that studied *C. elegans* with extrachromosomal arrays, control genotypes, which did not express the array, were obtained from siblings isolated from the same plates as nematodes that contained the array. *C. elegans* lifespan assays were conducted with animals grown on nematode growth media agar at 20°C in the presence of 40 μg/mL 5-fluoro-2′-deoxyuridine. All pathogenesis and lifespan assays were conducted with nematodes at the L4 larval stage. To obtain stage-matched animals at the L4 larval stage for the pathogenesis and lifespan assays, *olrn-1* mutant animals at the L1 larval stage were added to growth plates (NGM with *E. coli* OP50) approximately 24 hours before wild-type L1 larval stage animals were added to growth plates. Three trials of each pathogenesis assay were performed. Sample sizes, mean lifespan, and p values for all trials are shown in Table S2.

The propensity of *C. elegans* to avoid a small lawn (10 μL) of *P. aeruginosa* was determined by counting the number of *C. elegans* on or off the lawn at 4, 8, 16, 24 and 30 hours after synchronized L4 were placed on the bacteria (Foster et al., 2020). *C. elegans* development assays were performed as previously described (Cheesman et al., 2016; Foster et al., 2020). Brood sizes were quantified from five independent plates, each with two animals per plate. Animals were transferred to new plates each day to facilitate scoring of the progeny. Data for all replicates of the development and brood size assays are shown in Table S2.

Colony forming units of *P. aeruginosa* were quantified in the intestine of *C. elegans* as previously described with some modifications (Foster et al., 2020; Singh and Aballay, 2019). Briefly, *C. elegans* animals were exposed to *P. aeruginosa* for 24 hours. Animals were then picked to NGM plates lacking bacteria and incubated for 10 minutes to remove external *P. aeruginosa*. Animals were then transferred to a second NGM plate after which 10-11 animals per replicate were collected, washed with M9 buffer containing 25 mM levamisole and 0.01% Triton X-100, and ground with 1.0 mm silicon carbide beads. CFUs were quantified from serial dilutions of the lysate.

Generation of transgenic *C. elegans* strains

To generate *olrn-1* rescue lines, primers 5′-CAG AAC CAG ATT CTC GGA ATG A-3′ and 5′-AGA GGA AGA GAG ACA GGA TGA A-3′ were used to amplify the entire *olrn-1* locus. The resulting PCR product (30 ng/μl), the P*myo-3::mCherry* co-injection marker (15 ng/μl) and pBluescript SK (-) vector (155 ng/μl) were microinjected into *olrn-1(ums9);agIs44* animals to generate the arrays *umsEx4*, *umsEx6* and *umsEx7*.

The *olrn-1* neuron-specific rescue construct was generated using Gibson assembly to fuse 2kb of the *sng-1* promoter (amplified using primers 5′-CCC CCC CTC GAG GTC GAC GGT ATC GAT AAG CTT GAT ATC GTT GAG CAG CGA CTA ACA AAA-3′ and 5′-ACC TGA CAC TAA TTT CTC TTG GCG CTG AAC ATC TAG TCA TGC TAA AAT AAA AGA AAT ATA-3′) with 2960 bp of *olrn-1b* coding region + 667bp 3′ UTR (amplified using primers 5′-ATGACTAGATGTTCAGCGCC-3′ and 5′- GGC GGC CGC TCT AGA ACT AGT GGA TCC CCC GGG CTG CAG GTT TCA TAT ATC TTA TGC CGT −3′) in pBluescript vector linearized with *Eco*R1 (Gibson et al., 2009). The plasmid (30 ng/μl), the P*myo-3::mCherry* co-injection marker (15 ng/μl) and pBluescript SK (-) vector (155 ng/μl) were microinjected into *olrn-1(ums9);agIs44* animals to generate the arrays *umsEx20, umsEx21* and *umsEx23*.

Gene expression analyses and bioinformatics

For the RNA-seq experiment of *olrn-1(ums9)* and wild-type animals, synchronized L1 stage *C. elegans* were grown to the L4/young adult stage. RNA was isolated using TriReagent (Sigma-Aldrich), purified on a column (QIAGEN), and analyzed by mRNA-seq using the BGISEQ-500 platform (BGI Americas Corp). The quality of raw sequencing data was evaluated by FastQC (version 0.11.8) and Multiqc (version 1.7) (Ewels et al., 2016; Wingett and Andrews, 2018). Low-quality reads were trimmed using Trimmomatic (version 0.36) (Bolger et al., 2014). The trimmed reads were mapped to the *C. elegans* reference genome, WS220/ce11 [University of California Santa Cruz (UCSC) genome browser] using HISAT2 (version 2.1.0) (Kim et al., 2015; Pertea et al., 2016). The sequence alignment map (SAM) files were then converted to sorted BAM files using Samtools (Version 1.3.1) (Li, 2011; Li et al., 2009). The general transfer format (GTF) annotation file (WS220/ce11) was downloaded from the UCSC genome website, and the assembled GTF file was generated for each sample using Stringtie (version 1.3.4) (Pertea et al., 2015, 2016). Stringtie was then used to compare each sample against the merged assembly, estimate transcript abundance, and to generate a count table for Ballgown analysis (Pertea et al., 2016). The Ballgown package from the Bioconductor software suite (version 3.8) was used to run a custom R script in R console (R Version 3.5) to analyze the differential gene expression, visualize the data, and perform statistical tests for differential expression with multiple test correction. A gene was considered to be differentially regulated if its fold change versus wild-type was greater than two, the adjusted p value was less than 0.05, and its RPKM was greater than one.

To examine genes that are differentially expressed during *C. elegans* development, raw base-called fastq files were downloaded from the European Nucleotide Archive (accession number PRJEB31791). For each sample, reads were aligned to the WS220/ce11 on UCSC genome website using minimap2 (version 2.14-r883) (Li, 2018). Genomic alignments were run with the following parameters: -ax splice -k14 -uf -secondary = no -G 25000 -t 24. The resulting sam files were converted to bam format using samtools view with parameters: -b –F 2048 (Li et al., 2009). Read filtering and splice isoform identification were analyzed as described (Roach et al., 2019). The GTF (WS220/ce11) annotation file was downloaded from UCSC genome website and the assembled GTF file was generated for each sample using Stringtie (version 1.3.4). Stringtie was used to compare each sample against the merged assembly, to estimate transcript abundance, and to generate a count table for Ballgown analysis. The Ballgown package from the Bioconductor software suite (version 3.8) was used to run a custom R script in R console (R Version is 3.5) to analyze differential gene expression, visualize the data and perform statistical tests for differential expression with multiple test correction. Differential gene expression was defined as a fold change (FC) versus wild-type greater than 2, adjusted P value less than 0.05 and RPKM greater than one.

For the qRT-PCR studies, RNA was reverse transcribed to cDNA using the RETROscript Kit (Life Technologies) and analyzed using a CFX1000 machine (Bio-Rad) using previously published primers (Cheesman et al., 2016; Peterson et al., 2019; Troemel et al., 2006). All values were normalized against the control gene *snb-1*. Fold change was calculated using the Pfaffl method (Pfaffl, 2001). The analysis of *irg-4* and *irg-5* expression using nanoString was performed as previously described (Anderson et al., 2019; Cheesman et al., 2016; Pukkila-Worley et al., 2014). Counts from each gene in wild-type and *olrn-1(ums9)* animals were normalized to three control genes: *snb-1*, *ama-1* and *act-1*.

Immunoblot Analyses

Protein lysates from stage-matched *C. elegans* grown to the young L4 larval stage on *E. coli* OP50 on NGM agar were prepared as previously described (Cheesman et al., 2016; Peterson et al., 2019). Harvested animals were washed twice with M9 buffer, incubated in a roller at room temperature for 15 minutes to allow the nematode intestine to clear of bacteria, washed an additional time and flash frozen in RIPA Buffer (Cell Signaling Technology, Inc.) using an ethanol and dry ice bath. Samples were lysed by sonication and centrifuged. Protein was quantified from the supernatant of each sample using Bradford Reagent (Bio-Rad Laboratories, Inc.). Laemmli buffer (Bio-Rad Laboratories, Inc.) was added to a concentration of 1X and the total protein from each sample was resolved on Nu-Page 4%–12% gels (Life Technologies), transferred to nitrocellulose membranes (Life Technologies), blocked with 5% BSA in TBST and probed with a 1:1000 dilution of an antibody that recognizes the doubly-phosphorylated TGY motif of PMK-1 (Cell Signaling Technology), a previously characterized total PMK-1 antibody (Peterson et al., 2019) or a monoclonal anti-tubulin antibody (Sigma-Aldrich, Clone B-5-1-2). Horseradish peroxidase (HRP)-conjugated anti-rabbit (Cell Signaling Technology) and anti-mouse IgG secondary antibodies (Abcam) were used at a dilution of 1:10,000 to detect the primary antibodies following the addition of

ECL reagents (Thermo Fisher Scientific), which were visualized using a ChemiDoc MP Imaging System (BioRad). The band intensities were quantified using Image Lab software version 6.0.1 (BioRad), and the ratio of active phosphorylated PMK-1 to total PMK-1 was calculated with all samples normalized to the ratio of wild-type control animals.

Microscopy

Nematodes were mounted onto agar pads, paralyzed with 10 mM levamisole (Sigma) and photographed using a Zeiss AXIO Imager Z2 microscope with a Zeiss Axiocam 506 mono camera and Zen 2.3 (Zeiss) software.

QUANTIFICATION AND STATISTICAL ANALYSIS

Differences in survival of *C. elegans* in the *P. aeruginosa* pathogenesis assays were determined with the log-rank test after survival curves were estimated for each group with the Kaplan-Meier method. OASIS 2 was used for these statistical analyses (Han et al., 2016). qRT-PCR studies, lawn occupancy studies, intestinal CFU quantification, western blot band intensity quantification, and developmental assays are presented as the mean ± standard error. p values were calculated using one-way ANOVA in Prism 8 (GraphPad Software), unless otherwise indicated in the figure legend. Sample sizes, mean lifespan, and p values for all trials are shown in Table S2.

DATA AND CODE AVAILABILITY

The accession number for the mRNA-seq dataset reported in this paper is GEO:GSE130959. All other data are available in the manuscript.